LUT
Lappeenranta
University of Technology

Ilkka Korhonen

MOBILE SENSOR FOR MEASUREMENTS INSIDE COMBUSTION CHAMBER – PRELIMINARY STUDY

Thesis for the degree of Doctor of Technology to be presented with due permission for public examination and criticism in the Auditorium of the Student Union House at Lappeenranta University of Technology, Lappeenranta, Finland on the 15th of December, 2017, at noon.

Supervisors   Jero Ahola, D. Sc. (Tech.)
Professor
LUT School of Energy Systems
Lappeenranta University of Technology
Finland

Esa Vakkilainen, D. Sc. (Tech.)
Professor
LUT School of Energy Systems
Lappeenranta University of Technology
Finland

Reviewers   Lauri Sydänheimo, D. Sc. (Tech.)
Professor
Tampere University of Technology
Finland

Pasi Miikkulainen, D. Sc. (Tech.)
ANDRITZ Inc.
USA

Opponents   Anders Brink, D.Sc. (Chem.Eng.)
Professor
Faculty of Science and Engineering
Åbo Akademi University
Finland

Janne Väänänen, Dr. Tech (El. Eng.)
Docent
Finnpatent Oy
Finland

Abstract

Ilkka Korhonen
Mobile sensor for measurements inside combustion chamber – preliminary study
Lappeenranta 2017
102 pages

Acta Universitatis Lappeenrantaensis 779
Diss. Lappeenranta University of Technology
ISBN 978-952-335-180-6, ISBN 978-952-335-181-3 (PDF), ISSN-L 1456-4491,
ISSN 1456-4491

Large industrial boilers continue to grow in size. In the largest ones, the measurement systems no longer reach the inner parts of the combustion chambers. In addition, new measurement solutions are needed due to tightened regulations, new technology and use of renewable energy sources, such as biofuels. To measure in the inner parts of combustion chambers and to find new measurement methods, sensor ball propagating inside the combustion chamber was invented and patented. This research focused on the challenges in the implementation of such a sensor ball.

There are many technological issues to be solved before final use of the sensor ball. They concern communication possibilities inside the combustion chamber, the hovering of the sensor ball in different types of combustion, and the operating time of sensor balls in harsh environments such as combustion chambers and flames.

The preliminary research done and documented in this thesis concerns the following questions: What is the attenuation of radio and microwave signals inside the combustion chamber? What kind of electromagnetic noise is present in the chamber? What could be the operation time of a sensor in flames and what are the conditions for the hovering and propagation of the sensor ball inside the combustion chamber? Important issues such as receiving antennas, positioning of the sensor ball and feasible measurement solutions, which, can be interlinked with this kind of sensor, are mainly excluded from the study due to a lack of time and a need to limit the topic area.

The investigations done by calculations, modelling, simulations, and practical tests, yielded a number of results. First, the operation time of sensors balls in the boilers can be minutes. However, if the enclosure of the sensor ball is made from very good thermal insulation and the dissipation power of sensor electronics is not limited, the sensor can be destroyed more likely due to self-heating than an external high temperature. In addition, wires through the enclosure to sensor electronics can dramatically shorten the operation time of a thermally well-protected sensor. The hovering and free propagation of the sensor ball is possible in CFB boilers. If an operation time of about tens of seconds can be seen adequate, the sensor ball can also hover in many other types of boilers having adequate upward flows and suspension densities. Further, it was stated that communication is possible in the combustion environments, but demands special solutions. The main limitations to the communication are noise for wideband communication systems and

attenuation for all wireless systems. It was theoretically observed that at least in the combustion area of a kraft recovery boiler there exists weak plasma due to strong ionization originating obviously from alkaline.

As a preliminary result, it was seen that due to the effects of flames and ionization on the radio and microwave signals, the positioning methods and techniques, which are based on flight times and signal strength indications, do not suit the mobile sensor operating in the combustion area. In the combustion area, the sensor must position itself. The self-positioning solution is one of most important future research topics in parallel to e.g. the final communication solution and operating time extension.

Keywords: mobile sensor, combustion chamber, measurements, attenuation in flames, noise due to black body radiation, operation time.

Acknowledgements

To my nearest and dearest – to my family

Contents

Nomenclature

In the present work, variables and constants are denoted using *italics*, vectors are denoted using **bold regular font**, and abbreviations are denoted with regular font.

Latin alphabet

A	area	m^2
α	thermal expansion coefficient	$1/K$
B_v	Spectral radiance	$W/(m^2\ Hz\ sr)$
C_D	drag coefficient	–
d	diameter	m
ε	permittivity	F/m
$\varepsilon^{,,}$	imaginary part of permittivity	F/m
ε_0	permittivity of free space (absolute permittivity)	F/m
ε_r	real part of permittivity	F/m
F	force vector	N
G	Gain	
f	frequency	Hz
g	acceleration due to gravity	m/s^2
j	flux vector	m/s
k	heat transfer coefficient	$W/(m^2 K)$
k	Boltzmann's constant	
L	characteristic length	m
l	length	m
m	mass	kg
N	number of particles	–
n	refractive index	
n	unit normal vector	–
P	Power	W
p	pressure	Pa
q	heat flux	W/m^2
r	radius	m
S	total radiance	W/m^2
T	temperature	K
t	time	s
q_m	mass flow	kg/s
V	volume	m^3
v	velocity magnitude	m/s
v	velocity vector	m/s
W	energy	J
x	x-coordinate (width)	m
y	y-coordinate (depth)	m
z	z-coordinate (height)	m

Greek alphabet

α	(alfa)
β	(beta)
Γ	(capital gamma)
γ	(gamma)
Δ	(capital delta)
δ	(delta) notice the difference to ∂ (partial differential) symbol in equations
ε	(epsilon)
ϵ	(epsilon variant, Unicode 03F5, compare with equation symbol ϵ)
ζ	(zeta)
η	(eta)
Θ	(capital theta)
θ	(theta)
ϑ	(theta variant, Unicode 03D1, compare with equation symbol ϑ)
Λ	(capital lambda)
λ	(lambda)
∇	**(nabla) vector operator**
μ	(mu)
Π	(capital pi)
π	(pi) $\pi = 3.14159...$
ρ	(rho) density
ϱ	(rho variant)
Σ, Σ	(capital sigma)
σ	(sigma)
Φ	(capital phi)
ϕ	(phi variant, Unicode 03D5, compare with equation symbol ϕ)
Ø	(oh with stroke, Unicode 00D8, comp. with "empty set" in eq. symbols: $\emptyset$)
φ	(phi)
Ω	(capital omega)
ω	(omega)

Dimensionless numbers

Re	Reynolds number

Superscripts

p	partial layer
*	dimensionless

Subscripts

ds	dry solids
eff	effective
g	gas
s	solid
l	liquid
max	maximum
min	minimum
tot	total

Abbreviations

3D	Three dimensional
6D	Aix-dimensional (x,y,z, rotations)
AoA	Angle of arriving
AD	Analog to digital
BFB	Bubbling fluidized bed
BT	Bluetooth
CARS	Coherent anti-Stokes Raman spectroscopy
CCS	Carbon capture and storing
CFB	Circulating fluidized bed
dB	Decibel
dBm	Decibels proportioned to mW
ds	Dry solids
EM	Electromagnetic
FB	Fluidized boiler or bed
GSM	Global system for mobile communications
GPS	Global positioning system
HF	High frequency (band)
HHV	Higher heating value
HRSG	Heat recovery steam generator
IFRF	International Flame Research Foundation
IF	Intermediate bandwidth
IO	Input - output
IR	Infrared
ISM	Industrial, scientific and medical
KRB	Kraft recovery boiler
LDV	Laser Doppler velocimetry
LHCP	Left hand circular polarized
LHV	Lower heating value
LIF	Laser-induced fluorescence
LIP	Laser-induced phosphorescence
Ltd	Limited

MCR	Maximum continuous rating
MEMS	Micro electrical mechanical systems
MoEMS	Micro opto electrical mechanical systems
NOx	Nitrogen oxides
Np	Neper
PC	Pulverized coal, personnel computer
PCB	Printed circuit board
PCF	Pulverized coal firing
PFBC	Pressurized fluidized bed combustors
RHCP	Right hand circular polarized
PIV	Particle image velocimetry
RBW	Resolution band width
RDF	Refuse derived fuel
REF	Recovered fuel
RFID	Radio frequency identification
RSSI	Radio signal strength indication
RXD	Received data
SAW	Surface acoustic waves
SNR	Signal-to-noise ratio
SOx	Sulphur oxides
SPI	Serial peripheral interface
SWR	Standing wave ratio
TDoA	Time difference of arrival
TEM	Transverse electromagnetic
TOA	Time of arrival
TOF	Time of flight
TXD	Transmitted data
USB	Universal serial bus
UV	Ultraviolent
VBW	Video bandwidth
VIS	Visual light area
VHF	Very high frequency (band)
WLAN	Wireless local area network

1 Introduction

1.1 Background of the study

The research work and related theoretical study documented in this thesis started years ago. The basis for the work was set when Kari Saviharju, Director, Technology, at Andritz Oy Finland at the time, patented a mobile sensor for measurements in a closed space, meaning combustion chambers in large power plants [Saviharju, 2006]. Many years after the patenting, at a meeting considering measurement methods for combustion chambers, the idea for the mobile sensor in a combustion chamber was introduced to the author of this thesis. In the same meeting, the author was asked to start an investigation concerning boundary conditions and possibilities to develop the mobile sensor discussed. The work was to be a part of a comprehensive study concerning the behaviour and application of radio and microwaves in a combustion environment. In the "one man research group", the work was in practice compelled to focus on issues concerning the operation of a mobile sensor inside a combustion chamber.

Saviharju had discovered, as have many other combustion researchers after him, that many measurements in even larger boilers have been, are and will in the future be impossible to achieve with ordinary measurement solutions. These solutions are based on reaching, cooled probe structures carried in the boiler, typically for rather short-term usage (some hours) [Raiko, 2002; IFRF, 2009]. These types of cooled probes and suction probes can carry many different in-situ sensors, such as temperature, pressure, flow and ionization probes [Lackner, 2013; IFRF, 2009], and sampling devices inside the furnace for taking chemical samples [Halpern, 1958]. The probes are cumbersome to use, heavy, expensive and susceptible to damages. In addition, the water cooling of probes can be risky; water leakages from the probe to e.g. the operating kraft recovery boiler can generate a so-called smelt-water explosion. For combustion suspension, flow and other measurements, there are optical measurement systems (laser Doppler velocity (LDV), particle velocity velocimetry (PIV), coherent anti-Stokes Raman spectroscopy (CARS), laser-induced phosphorescence (LIP), laser-induced fluorescence (LIF), pyrometry, etc.) [Raiko, 2002; Kohse-Höinghaus, 2002; Lackner, 2013; Webber, 2000; Rogalski, 2014]. Optical devices must be accompanied by measurement positions because with remote measurements it is difficult to know which sampling positions the results actually represent. An exception exists: in kraft recovery boilers, the infrared cameras enable monitoring the shape of the char bed at the bottom of the boiler visually.

The behaviour of radio and microwaves inside combustion chambers has been very little investigated. Still, there are some papers concerning the issue. Some of them deal with the pre-treatment of fuels, e.g. coal by microwaves [Binner, 2014; Zuo, 2016]. There are temperature sensing, flow and density measurement and tomographic profile measurement applications. [Stephan, 2004; Hauschild, 1995; Williams, 2006]. However,

most of research work has been done in a laboratory environment in test systems of very small dimensions. So, all results are not directly scalable to measurements in industrial-scale boilers.

There is one principal problem in all boilers concerning measurements, not only radio and microwave based measurements: in the walls and roof of the boilers, there are very little or no openings for measuring devices and antennas. The openings are typically very small in size. This means that only microwave based measurements are possible in the combustion chambers. The second problem is the harsh environment containing aggressive chemicals causing corrosion and disturbing measurements. Further, grinding particles cause erosion especially in fluidizing bed boilers.

As stated above, boilers are becoming even greater in size. The largest boilers have bottom areas of many hundred square meters and their heights are varying from 60 to 90 meters. Regulations concerning emissions and pollution originating from industrial energy production are tightening. Typical pollution monitored and controlled includes carbon oxides (CO_2, CO), nitrogen compounds (NO_x and N_2O), ozone (O_3), and sulphur oxides (SO_x) [Raiko, 2002, Lackner, 2013]. In addition, air toxics and trace metals in ashes are under even stricter monitoring. [Lind, 1999; Ljung, 1997]. Considering owners and investors, better economics or more profitable overall usage of boilers is called for. Summarizing all technical and economical requirements, there is a clear need for new measurement techniques. A mobile sensor ball could be one solution. Its idea is to complement measurement techniques in use today and to extend measurements to all parts of the furnaces.

1.2   The aim of the study

The scope of research work is to gather background information for understanding microwave based measurements inside combustion chambers and developing a mobile sensor or sensor ball capable of propagating, measuring and relaying measurement information in a combustion area (flames) to a so-called base station outside of the combustion chamber; see Figure 1.1.
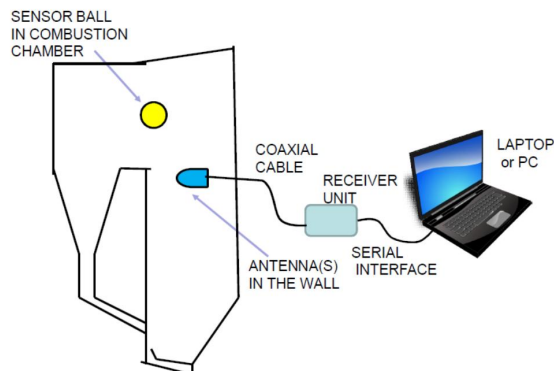
Figure 1.1: Principal elements considered in the study: combustion chamber, sensor ball and communication link. In addition, data collection and analysis tools on a laptop or personal computer (PC) are included to the system.

The sensor ball will be disposable. Consequently, it must be sufficiently low-cost so that many sensor balls can be used to obtain holistic results for a measurement case. The sensor ball consists of sensor electronics and a cover. The sensor electronics have active microprocessor based core and interface circuits, a serial peripheral bus (SPI) bus and a digital input-outputs (IO) for sensors. The main sensors are internal and external temperature sensors. In addition, the sensor electronics includes a radio module and an internal antenna for communication. For positioning, the sensor electronics will include a 6D Micro Electrical Mechanical Systems (MEMS) element capable of measuring accelerations and rotations in three directions (axes). The sensor electronics is powered by a battery. The duty of the cover is to delay the rise in temperature of sensor electronics in a high temperature environment and to protect sensor electronics from dust, sand and other particles. The cover also protects the sensor electronics from mechanical shocks.

The sensor is led to the combustion chamber where it propagates and measures process parameters, such as the temperature, pressures, flows, and perhaps one day in the future, chemical compounds and e.g. ionization. The sensor sends the information it is collecting, including position data, by radio link to an antenna or antennae in the walls of the combustion chamber. The antennae are connected to receiver units, which decode radio messages and send information to a laptop or PC via a serial or Ethernet link. The software running on the laptop or PC stores the information and shows it in a format later defined. The information contains both process values and positioning data.

Before a mobile sensor capable of operating in furnaces can be physically implemented, many issues must be investigated in detail. These are communication in a fire environment, starting from noise and attenuation, hovering conditions for the ball in different boilers, the operation time of the sensor and thermal insulators suitable to protect

the sensor ball in the combustion environment, and positioning the sensor ball. In addition, measurement methods and techniques must be defined and implemented.

The greatest challenge in developing the mobile sensor depicted above cannot yet be defined. At first glance, it seems that all issues in the background present a great challenge. Whatever the truth, this study discusses some of the current technical challenges relating to the sensor and gives preliminary solutions with theoretical and experimental data to most of them.

The lifetime or operation time of the sensor is a key issue in the research. The extreme conditions inside boilers demand solutions which differ from ordinary sensor and measurement technologies. High temperatures have a great impact on the lifetime of the sensor. Corrosive and erosive flows and chemical compounds have their own effects on the solution, although corrosion itself is not such a significant issue for short-term sensor operation. The research explores background issues related to the sensor's operation, from introducing boilers and fuels to the modelling and experimental testing of the lifetime of prototype sensors. One of the main issues studied was the capability of technical insulators to protect sensor electronics.

Combustion chambers are problematic for measurements and communications not only due to their high temperatures. A mobile sensor should send all measurement information or process values and position information to the base station. A radio or microwave link is used for the purpose. The chemical suspension and flows in the chambers strongly affect the radio and microwaves used inside the chambers. Especially alkaline originating from biomass and equivalent fuels strongly impacts communication due to ionization. The study determines limitations of wireless communication inside combustion chambers.

To connect the measured process values to the locations where they were taken inside the combustion chamber, the sensor ball must positioned. This thesis does not deal with the positioning. However, as a preliminary research result, the positioning of the sensor ball cannot be based on positioning techniques typical of mobile sensors in ordinary environments. These methods, based typically on the flight time of the signal or signal attenuation on the propagation path, will in the combustion environment suffer from unstable, intangible signal path properties introduced later in this document. Furthermore, Global positioning system (GPS), which is the most common way to position mobile devices outside and globally, is completely non-operational in a closed, electromagnetically noisy combustion chamber. The positioning must be based on self-positioning or on anchor techniques suitable for the indoor positioning of small mobile devices [Savarese, 2002]. The latter is not discussed in this thesis.

The electronic solution to the sensor platform poses no exceptional challenge to the research. There are many possible platforms available for prototyping. However, the electronics sensors capable of operating in connection to a mobile sensor platform raise interesting research and practical questions, which this thesis will briefly discuss.

Last, but not least, are issues relating to the propagation of a sensor ball inside a combustion chamber. The sensor ball will have no active means to control its trajectories inside the chamber. The flows in boilers and the consequent drag forces, and to some extent buoyage or the buoyant force, will define the propagation of the sensor ball.

1.3   Structure of the study

This thesis starts with a theoretical study of issues relating to the research of mobile sensors operating in a combustion chamber.

Chapter 2 presents typical boiler types and some details of their technical implementation, focusing on boiler properties and operation. In addition, chapter 2 includes a short description of fuels, mainly pointing out features which impact first and foremost the propagation of radio and microwaves inside the combustion chamber.

In the chapter 3, the electromagnetic theory is introduced as the basis for studying the communication, measurement and positioning means of the sensor. Study of propagation of electromagnetic waves in lossy materials prefaces the behaviour of electromagnetic waves in combustion area. The electromagnetic studies focus on radio and microwaves.

Chapter 4 examines the behaviour of radio and microwaves inside the combustion chamber. The aim is to understand the communication possibilities inside the chamber. The chapter includes both attenuation and noise related information based on the theory and measurements in a Kraft recovery boiler (KRB).

In chapter 5, operating time issues are discussed. First, the possibilities to use high temperature electronics in sensor solution is studied. Operation time of a sensor in combustion area is strongly related to high temperatures in combustion chambers and properties of insulating materials used to protect sensors and extend the operating time of the sensors. Some insulation materials are introduced, and operation times of sensor balls made from them are modelled, simulated and tested in a small combustor. Hovering issues are partly included in this chapter because the mass of the enclosure insulator of the sensor ball plays an important role in hovering questions. In the chapter, the test sensor and its electronics used in the first tests are introduced, too.

Chapter 6 studies the propagation of the sensor ball inside a combustion chamber. The main issues are the hovering conditions. If the ball does not hover in a combustion chamber or parts of it, it cannot propagate inside the chamber. The hovering of the sensor is closely related to the mass and cross-section of the sensor ball and to the conditions inside the combustion chamber, such as flows and suspension densities. The hovering was studied by modelling and calculating the hovering conditions of similar sensor balls used in operating time tests and modelling.

In chapter 7, the next generation of the sensor electronics is tentatively outlined based on information gathered from the research work. In addition, new measurements with sensor ball are surveyed.

Chapter 8 discusses the research of radio and microwaves and the implementation of the sensor ball. Finally, in chapter 9, conclusions are drawn.
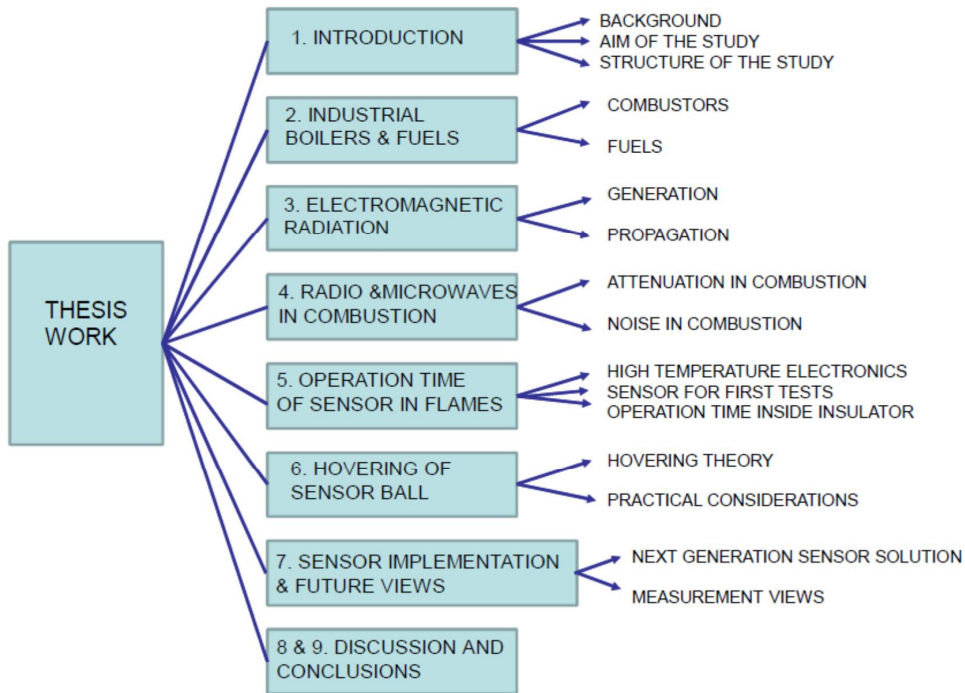
Figure 1.2: Structure of the book

2 Industrial boilers, fuels and combustion processes

There is various industrial boilers for power and recovery usage. Because conditions in combustion chambers strongly affect sensor ball propagation and measurements, the next sections provide an overview of boilers and fuels.

2.1 Boilers

Many types of combustion boilers are available for industrial or district heating usage. The main purpose of these boilers is power production by changing chemical energy bound to fuels into thermal energy. [Raiko, 2002]. Recovery boilers have dual duties. They are intended for both power production and chemical recovery. Figure 2.1 provides a classification of combustion based power plant types:
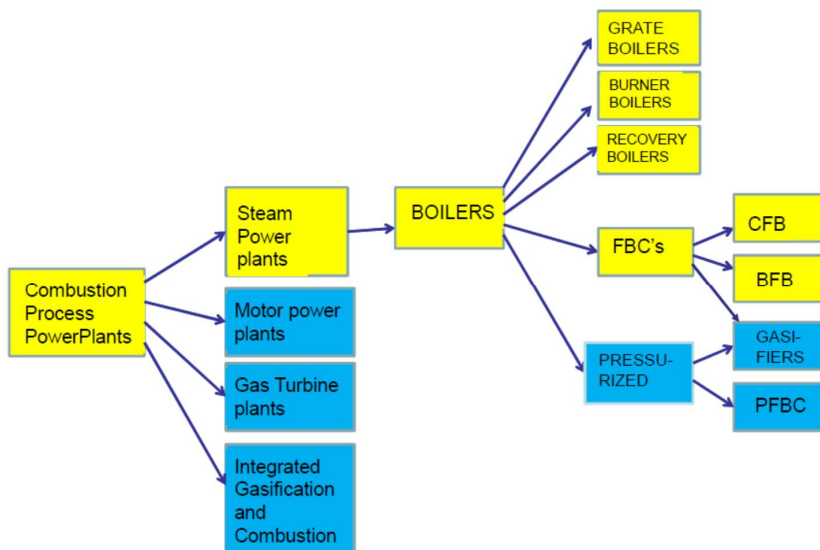
Figure 2.1 : A classification of combustion based power plants. The thesis focuses on elements marked with yellow.

The most common industrial thermal power source is the steam boiler. Steam is generated in grate and fluidizing bed combustors using gas, oil, (pulverised) coal, peat, wood and biomass in many forms as an energy source. In kraft recovery boilers, black liquor is the main fuel. Many combinations of fuel supply and combustion techniques are available.

Most boilers have water-steam loops for cooling the boilers and transporting thermal energy forward from the boiler. Steam or hot water is used e.g. to energise turbines or to

heat the industrial process around the power plant or for district heating. Further, all boilers have high combustion temperatures up to 1400 ºC; see Figure 2.2. Temperature profiles differ slightly from one boiler type to another. [Teir, 2003]. In addition, all combustion processes contain aggressive gas mixtures causing corrosion and slagging of the boilers and structures inside the chambers due to sticky particles in gas suspensions. Because different boilers have their special structures and combustion processes, they are each briefly described below.
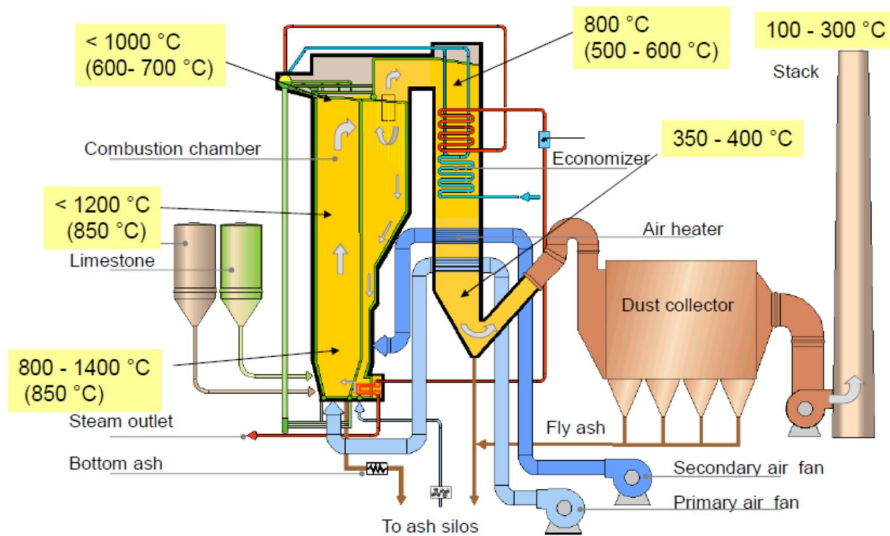
Figure 2.2: Example of modern steam boiler (circulating fluidizing bed or CFB) with auxiliary equipment. Temperature values typical to boilers, except CFB boilers, for which temperature values are given in brackets. Modified after [Hultgren, 2014].

2.1.1   Grate boilers

Grate boilers represent the oldest boiler type. Grate boilers typically have a fixed or moving grate onto which the fuels are supplied for combustion. Only solid fuels, such as biomass and coal, can be burned in grate boilers. The air for the combustion process is blasted through the grate. Grate boilers are quite common in small municipal power plants. Because the operation of grate boilers is not very dependent the material size and size distribution, they are quite often used in waste combustion. [Cyranka, 2016]

2.1.2   Fluidized bed boilers

Fluidized bed boilers burn fuels in a particular mode of solid-gas contacting. Therefore, fluidized bed combustors efficiently combine a combustor and heat exchangers, enabling a highly controllable and intrinsically stabile combustion process.

The idea of fluidizing combustors is based on the usage of a bed consisting of granulate, small unburning particles, typically sand particles. In the combustor, the primary air supply is at the bottom of the boiler vessel. When the air supply is started and increased, the bed sand will become thinner. The voidage of the bed is increasing. When the air supply is increasing, the sand bed starts to bubble and then fluidize. Behaving as a fluid, it no longer has exact forms and directions. When the air supply is sufficient, the sand rises tens of meters and returns to the bed on the walls of the combustion chamber or in a back-loop intended to restore the circulating sand (Figure 2.3).
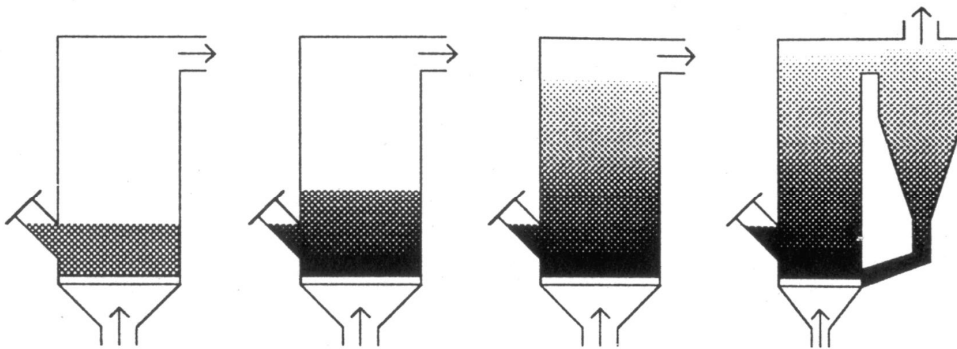
Figure 2.3: Fluidizing degrees: static bed, void bed, bubbling bed and circulating bed. [Raiko, 2002]

The usage of sand evens the combustion process by acting as a buffer of energy e.g. when variations in the moisture or heat values of the fuels vary. According to the behaviour of the sand bed, the fluidized bed combustors are divided into two classes: bubbling fluidized bed (BFB) and circulating fluidized bed (CFB) boilers. In BFBs, the heat is transported to the boiler walls mainly as hot gas convection and heat radiation. In CFB boilers, heat is transported by circulating sand and ash, which also even out the combustion temperatures and processes in the riser area of the combustion chamber; see Figure 2.2. Temperature values of about 850 $^{\circ}$C in the riser area mean less NO_x and N_2O pollution compared to higher or lower temperatures.

 Figure 2.4 and Figure 2.5 show the bed and suspension density profiles inside the combustion chambers.
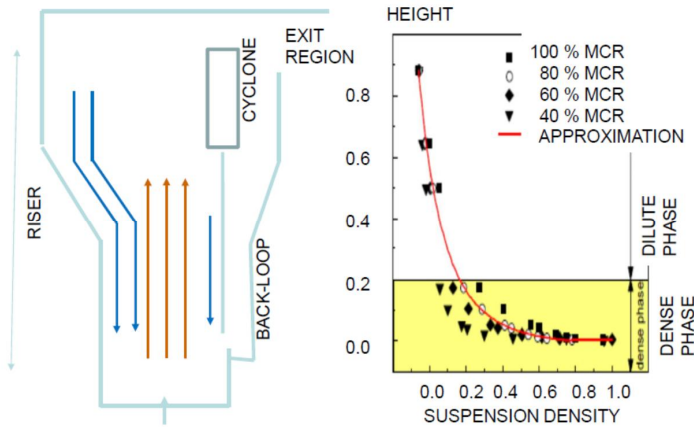
Figure 2.4: Flows in CFB boiler and suspension density profile inside the CFB boiler. [Tourunen, 2013]

In CFB boilers (Figure 2.4) in the middle parts of the riser area, the suspension flows containing sand, ash and fuel fractions go upwards (red arrows in Figure 2.4). In the flows, suspension densities can rise up to 10-30 kg/m^3 in riser top areas and much more at lower levels. The sand/ash returns to the bed area through a back-loop and near and along the walls of the riser area (blue arrows). On the bed, the density is about 10-100 kg/m^3. The mean gas velocities in the boilers are 4-6 m/s [Basu, 2006]. Some give wider velocity areas, such as 3-10 m/s [Huhtinen, 2004].
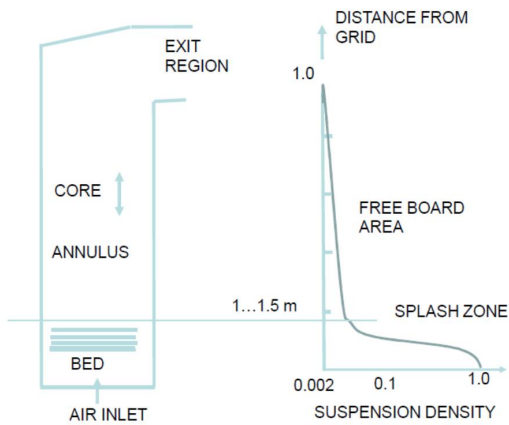
Figure 2.5: Suspension density profile inside the BFB boiler.

In the free board area in BFB boilers, the amount of sand particles is quite small, and so, the suspension density is of the order of gas mixture densities, 0.4- 0.6 kg/m^3. The density of the bed is about 1200-2400 kg/m^3; see Figure 2.5. The suspension flow rate is about 0.5- 2.5m/s in BFB boilers. [Basu, 2006; Huhtinen, 2004]

The circumstances inside the CFB and BFB boilers are extremely harsh for both the boiler structures and measuring devices assembled or existing inside the chambers. In addition to extremely high temperatures and aggressive chemical gases and substances typical to all boilers, the fluidizing material or sand particles in all densities cause grinding of structures inside the chamber.

2.1.3   Pulverized coal firing (PCF)

Pulverized coal is undoubtedly the most common solid state fuel. Coal has traditionally been burned in grate boilers and is still burned in small volumes. At present, most of the coal is burned in pulverized form. After grinding and drying, the pulverized coal is fed with air into the combustion chamber by special burners. The pulverized coal is in small granulate form about 75-95 µm in diameter. [Yeh, 2007; Teir, 2003].

The thermal power of PCF boilers exceeds 1000 MW [Franke, 2003]. The net plant efficiency of supercritical coal boilers is up to 42-44 %. The amount of PCF boilers is still increasing [Hachenberg, 2014].

2.1.4   Recovery boilers

Recovery boilers recover chemicals or inorganic elements from fuels and produce energy from organic parts of fuel. The most common recovery boiler is a kraft recovery boiler, which is a significant element in chemical wood processing. KRBs use black liquor as fuel. The water content of black liquor, when dried for spraying into combustion, is quite high: 15-30 % [Teir, 2003]. The lower heat value (LHV) of the material is around 12-13 MJ/kg in dry solids (ds) [Teir, 2003]. Despite that, recovery boilers produce most of the steam and power needed in pulp and paper mills.

The gas suspensions in KRBs differ substantially from those e.g. in CFB and BFB boilers burning coal, peat or wood chips. The main difference is in the alkaline originating from black liquor, which contains potassium (1.0 % ds) and sodium (19.9 % ds). The high alkaline and sulphur (4.8 % ds) concentrations cause severe slagging, fouling and corrosion [Vakkilainen, 2007]. Alkaline content is important because it increases chemical ionization due to low activation energies [Boan, 2009]. This, in turn, can have, as will be stated later in this document, a strong effect on signal attenuation inside the combustion chamber.

The suspension densities in the middle parts of kraft recovery boilers are not well defined in literature. They consist of gas mixtures, fume particles and unburnt char bed particles. The fume particle densities in the top areas are 16- 35 g/m^3 according to Samuelsson [2012] or 14-32 g/Nm^3 according to Mikkanen [2000]. Added to gas mixtures, the total densities in the top parts of KRBs are about 296-318 g/m^3. The density of the char bed area varies from top to bottom: active zone 290-496 kg/m^3, inactive zone 480-1330 kg/m^3, molten smelt 1923 kg/m^3, and solidified smelt 2163 kg/m^3. [Adams, 1988]

2.1.5   Summary of boilers

There are numerous types of boilers in the world. In addition, many cross-technologies combine the best features and benefits of each basic type; see Table 2.1.

Table 2.1 Summary of basic boiler types [Basu, 200; Utt, 2011; Vakkilainen, 2007]

ITEMS	Grate boilers	BFB boilers	CFB boilers	PCF boilers	KRB boiler
Height of the bed of the fuel zone (m)	0.2	1 – 2	15 - 40	27 - 45	40 - ~ 80 m
Flue gas velocity m/s	1.2	1.5 – 2.5	4 - 8	4 - 6	3 – 5
Excess air %	20 - 30	20-25	10-20	16 - 30	15 – 20
Grate/bottom heat release rate MW/m^2	0.5 – 1.5	0.5 – 1.5	3 -5	4 -6	2.7- 4
Temperature area (ºC)	800-1100	800-1000	850-900	1300-1400	1100-1300
Fuel "chip" /droplet size mm	32-6	6-0	6-0	<0.1	5 – 12
Turn down ratio	4:1	3:1	3 - 4:1	2:1	2:1
Nitrogen oxides (NO$_x$) ppm	400 - 600	300 – 400	50 - 200	400 - 600	200- 400 mg/Nm^3
Sulphur dioxide capture in furnace %	None	80 – 90	80 – 90	>90	99
Combustion efficiency %	85 - 90	90 – 96	95 - 99	99	98

All combustion chambers have metallic walls, which limit the combustion area and exchange thermal energy. The walls collecting thermal energy are typically so-called tube walls. The metallic walls can be partly or completely covered with concrete or brick structures that provide protection against excessive heat.

The circumstances inside combustion chambers are extreme. High temperatures, strong chemicals and grinding suspensions wear the metallic and other structures in combustion chambers. Slagging and fouling decrease heat exchange and coat small structures, such as sensors and antennas, on the walls [Basu, 2006; Zbogar, 2004]. Consequently, combustion chambers in any boiler are a challenging environment for measurements and sensors.

2.2   Fuels

The burning processes are characterized by boiler technologies and fuels used in burning. Because the properties of fuels affect measurement and communication techniques used inside the combustion chamber, fuels are briefly examined here.

Fuels are classified into two main groups: fossil fuels and renewable fuels. Fossil fuels have accumulated into the ground millions of years ago. Renewable fuels are produced from renewable sources, such as plants, the sun or wind. Combustion in industrial boilers is mainly based on reactions of hydrocarbons, which consist of carbon, hydrogen and oxygen elements. In addition, fuels contain varying amounts of elementary compounds, such as nitrogen (N), potassium (K), sodium (Na), and sulphur (S), and trace metals, such as chrome (Cr), mercury (Hg), nickel (Ni), and cadmium (Cd) [Vouk, 1983]. The usability of fuels in terms of environmental and boiler reliability is defined by additives and trace materials. The combustion of any fuel produces carbon monoxide (CO), carbon dioxide (CO_2) and nitrogen oxides (NOx). Some elements, such as sodium and potassium, and many alkaline compounds, such as K_2O, Na_2O and CaO, can cause erosion and corrosion in the boilers [Khan, 2009]. They can also impact the behaviour of electromagnetic waves in combustion area significantly. In addition, moisture has an impact on electromagnetic waves in the form of absorption at certain wavelengths.

2.2.1   Elementary compounds in fuels

In addition to elementary coal sulphur, coal and its derivatives contain nitrogen, hydrogen and oxygen. Ash and trace metals in coal make the exploitation of coal difficult [Vouk, 1983]. Also other fossil fuels, such as crude oils, shale oil and gases, contain additives. As an example, oils contain sulphur ranging from 0.5 to 6.0 % [Demirel, 2012].

Natural gas is mostly methane (CH_4) – up to 96 %. In addition, it may contain nitrogen (N) in amounts varying from 0.7 to 5.6 %. The content of counterproductive compounds is very low in the gas.

Renewable fuels are biomasses, liquids produced from them and directly from plants, and gases produced from biomass. The ash of biomasses contains many free and bound elements. They are, in decreasing order, C, O, H, Ca, K, Si, Mg, Al, S, Fe, P, Cl, Na, Mn and Ti [Vassilev, 2013]. The ash content of biomass can vary from 1.37 weight-% in willow (Salix) tree to 5.7 weight-% in wheat straw [Hurskainen, 2013] and 7.7 % in foliage of Scandinavian trees [Werkelin, 2005]. There are also species with a very high ash content, such as rice straw with an ash content of 19.17 % ds [NREL, 1997]. The percentages of these elements vary greatly between biomasses: for example, the sodium contents can be about 0.5 % ds and potassium content up to 3.4 w.-% of the dry weight [Hurskainen, 2013]. Further, according to Wang [2013], the CaO content of wheat straw

is 6.10 % ds, the K_2O content 29.9 % ds and the Na_2O content 1.10 % ds, and the figures for saw dust are 26.13 % ds, 14.47 % ds and 11.37 % ds, respectively.

In domestic tree species, such as pine, spruce, birch and aspen, the calcium (Ca) content can be 410-1340 ppm in the wood part and 4800-19100 ppm in the bark. The potassium (K) content varies from 200 to 1310 ppm in the wood part and from 7100 to 25000 ppm in the young foliage. Chlorine (Cl) can vary between 30 and 110 ppm in the wood part and 330 ppm in the bark part. Sulphur (S) amounts can vary from 50 to 200 in the wood and from 5000 to 11300 in the needles. [Werkelin, 2005]

Apart from alkaline, sulphur (S) and chlorine (Cl) compounds, small amounts of trace metals, such as arsenic (As) and cadmium (Cd), are present in the tree species. Alkaline and trace metals can cause both severe air pollution and strong corrosion and slagging in combustion chambers. Small concentrations of cadmium in wood ash prevent the spreading of ashes back into the nature. [Hansen, 2001]

Biofuels can be cultivated oils, such as turnip, rape or palm oil, or wood based residuals and original wood oils [Batidzirai, 2013]. The most frequently used residual liquor is black liquor, which is a by-product of pulp cooking. Black liquor comprises a diverse set of organic and inorganic elements and compounds; see Table 2.2.

Table 2.2: Consistence of black liquor made from birch. [Söderhjelm, 1994]

Element/compound	% of dry solids	Element/compound	% of dry solids
ORGANIC COMPOUNDS	78 %	**INORGANIC COMPOUNDS**	22
Lignin	37.5	NaOH	2.4
Hemicellulose	22.6	NaHS	3.6
Aliphatic acids (lignin, carbohydrate)	14.4	Na_2CO_3 , K_2CO_3	9.2
Fatty acids, resin acids	0.5	Na_2SO_4	4.8
Polysaccharides	3.0	Ns_2S_2O and Na_2S	0.5
		NaCl	0.5
		Other elements (Si, Ca, Mn, Mg, etc.)	0.2

The organic part of black liquor is burned for energy, and the inorganic parts, such as potassium and sodium, are recovered for a new pulp cooking cycle [Vakkilainen, 2007].

Peat contains quite an amount of heavy metals and other harmful elements [Tulonen, 2012].

All fuels made from waste are challenging to burn because of variations in the significant moisture and foreign matter contents between waste lots [Steenari, 1999]. The ash composition of wood waste is rather constant, which is typical of woods, but e.g. waste from sewage sludge has different compositions: silicon dioxide (SiO_2) 26.36 % ds, aluminium trioxide (Al_2O_3) 31.74 % ds, calcium trioxide (CaO) 13.08 % and phosphorous pentoxide (P_2O_5) 16.96 % ds. Especially chlorine, originating from plastics, in RDF demands good burning conditions and monitoring of flue gas contents. The chlorine content can be about 5.8 % of the RDF total mass [Penque, 2007].

3   Electromagnetic radiation

Electromagnetic waves, especially radio and microwaves, can be used in two ways in combustion area measurement techniques: First, electromagnetic waves can be used in the direct measurement of fire operation or in the indication of e.g. special chemical elements and compounds. This happens e.g. in all optical measurement techniques used in combustion measurements [Rogalski, 2014; Kohse-Höinghaus, 2002; Webber, 2000]. Some studies and applications are based on radio and microwaves to direct measurements on combustion phenomena [Stephan, 2004; Stockman, 2009]. Secondly, radio and microwaves as part of electromagnetic waves can be used for communication and for the positioning of the sensor inside combustion chamber. This thesis studies the use of radio and microwaves in communication inside a combustion chamber. This chapter introduces electromagnetic waves and their behaviour in free air and a free medium. The main topics of the chapter are the noise and attenuation of an electromagnetic wave. The focus is on the microwave frequency area.

Electromagnetic radiation is a ubiquitous phenomenon which appears in the form of self-propagating waves in the matter and vacuum. Electromagnetic radiation can be conceptually described as waves or particles. The waves consist of a series of crests and troughs, ups and downs, sequentially. The distance between adjacent crests or adjacent troughs is called the wavelength (λ) of the radiation. The frequency (f) defines the repetition rate of crests or troughs. These two parameters are in close relation to each other:

$$v = \lambda f \qquad\qquad\qquad (3.1)$$

The propagation speed v of the electromagnetic wave in a free space (air) is c $\approx$ 300 000 km/s. Substituting v by c in the equation above, we get absolute values between the wavelength and frequency in a free space.

When electromagnetic radiation is described in the form of particles or as small energy packets, they are typically called photons or quantum [Woodhouse, 2006]. The energy of a quantum is

$$W = h f \qquad\qquad\qquad (3.2)$$

in which h is Planck's constant $6.6256 * 10^{-34}$ Js.

In a free space, electromagnetic radiation propagates as a transverse-electric-magnetic (TEM) wave, in which the vectors of electric and magnetic fields are perpendicular to each other and the direction of the propagation.

The spectrum of electromagnetic radiation is very wide, ranging from a few thousand hertz at a low radio frequency and extending up to the 10^{18} hertz frequency of gamma rays (Figure 3.1). In the middle of the logarithmic scale of electromagnetic waves, there is a very narrow area of visual light. Near the visual light (VIS) band, at slightly lower frequencies, exists the area of infrared light (IR), the other area of the electromagnetic spectrum, which human senses (skin nerves) can observe. Between microwaves and optical spectrum areas (IR, VIS and ultraviolet (UV) areas) there is the rarely applied, but very interesting terahertz area. This area is under intensive research, and some products are already available for use at this band.
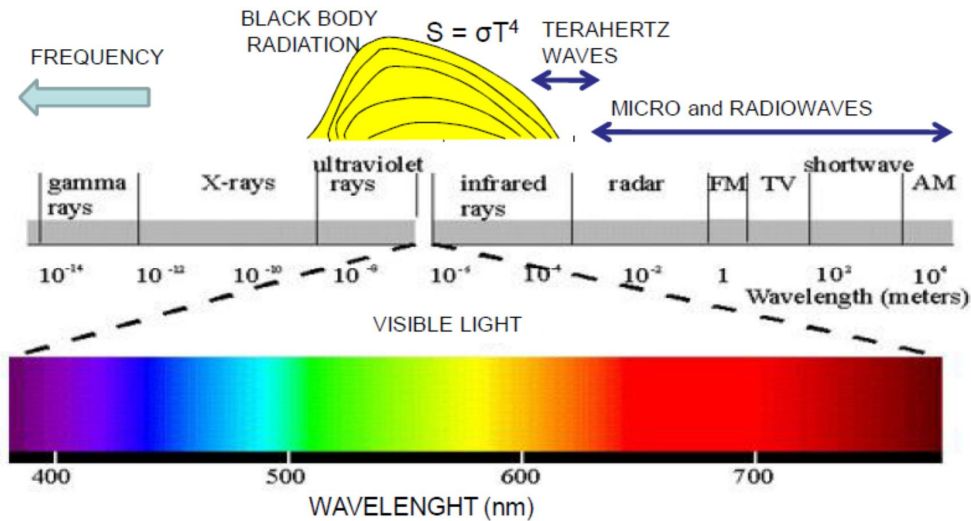
Figure 3.1. Electromagnetic spectrum. The black body radiation (see 3.2) area is shown in the middle of the figure. Original picture [Coworker, 2017].

In the combustion environment, the electromagnetic spectrum emphasizes the infrared (thermal radiation), visible light, ultraviolet area. However, it can be seen that the total spectrum is much wider because of many molecular and atomic level phenomena present in the flames. The electromagnetic spectrum inside the combustion chamber caused by external sources appears quite small because the metallic and concrete based structures strongly attenuate the electromagnetic radiation in both directions: inward and outward from the combustion chamber. However, this information must be considered merely preliminary because of the lacking measurement and research information.

3.1   Electromagnetic field in free space and medium

The relationship between time-varying magnetic and electric fields and the medium are described by Maxwell equations. In the following, they are introduced in time-harmonic form, in which the angular speed $\omega = 2\pi f$ and $j\omega = \partial/\partial t$.

$$\nabla * \vec{E} = \frac{\rho}{\varepsilon} \tag{3.3}$$

$$\nabla * \vec{B} = 0 \tag{3.4}$$

$$\nabla \times \vec{E} = -j\omega B = -j\mu\omega\vec{H} \tag{3.5}$$

$$\nabla \times \vec{H} = J + j\omega D = J + j\omega\varepsilon\vec{E} \tag{3.6}$$

where E is the electric field (V/m), H is the magnetic field (A /m), B is the magnetic flux density (T), D is the electric flux density (C/m), J is the electric current density or displacement current, ρ is the electric charge density (C/m^3), ε is the permittivity of the medium (F/m or C/ Vm) and μ is the permeability of the medium (H/m or Vs/A).

Equation (3.3) describes with divergence operator "$\nabla*$" that the electric field is source based and it has a tendency toward divergence. The electric field is charge density divided by permittivity ε, which in free space equals 1. Equation (3.4) in turn claims that the magnetic field is sourceless or there exist no magnetic charges. Therefore, the divergence of the magnetic field is zero. Equation (3.5) shows that a changing electric field generates a changing magnetic field, and the fields are diagonal. The curl operator "x" describes the curling of the magnetic field. Equation (3.6) means that a changing magnetic field generates the electric field and displacement current J. It describes the change of the electric displacement field.
Permittivity ε describes the ability of a dielectric material to polarize as a response to the electric field. It thus defines how the electric field is affected by the material and vice versa. The greater the permittivity is, the lower electric field inside the material is as response to the external electric field. The value of the permittivity varies inside the material with the temperature, moisture, orientation and pressure. The medium, in which permittivity depends on applied field, is called nonlinear material.
Complex permittivity is defined to describe the frequency dependence and behaviour of permittivity in the material. Complex permittivity is defined in equation (3.7.)

$$\varepsilon = \varepsilon_r(\omega) - \varepsilon''(\omega) \tag{3.7}$$

The real part (ε_r) describes the storage properties of the material and the imaginary part (ε') absorption or loss related properties of the material. Consequently, for the lossless dielectric medium, the permeability is real (ε_r). The frequency dependence of complex permittivity is shown in Figure 3.2.
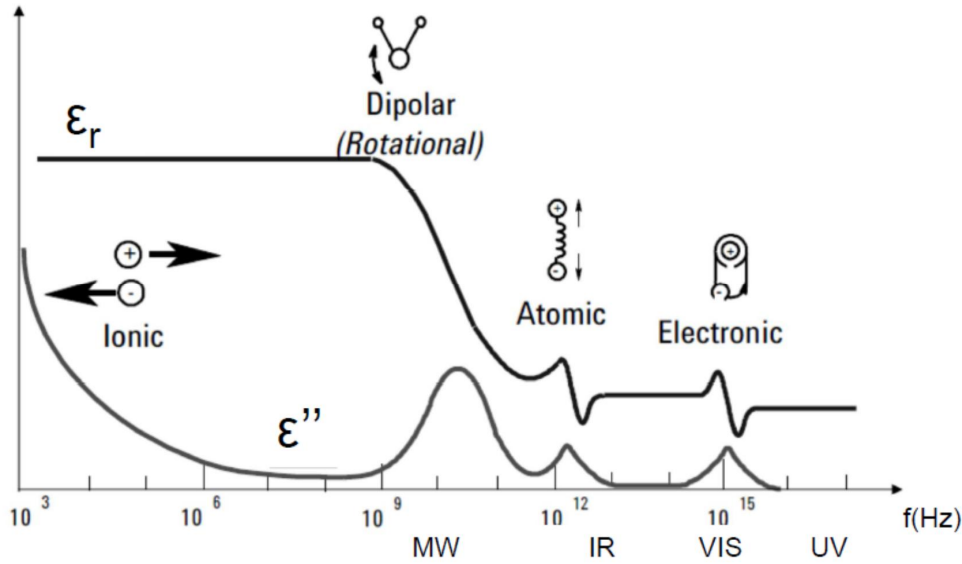
Figure 3.2: Complex permittivity as a function of frequency [Agilent, 2006].

The real part of permittivity remains stable up to frequencies of about 10^9 Hz. At higher frequencies, at the gigahertz level, atom or molecule resonance related peaks are detected. At even higher frequencies, electron or orbit level resonances are detected. The imaginary part describes losses, which decrease from small frequencies up to megahertz. At higher frequencies, strong peaks are detected. At frequencies of about 10^{15} Hz, the UV region and further, the electromagnetic energy is fully absorbed by atoms, exciting electrons to upper the energy levels. Consequently, ionization and ionizing radiation occur at these frequencies.

The permeability of material describes the capability of the material to support the formulation of the magnetic field in the material. It defines the magnetization of the material as a response to the magnetic field.

Generally, permittivity and permeability μ define the refractive index (n) of a material. In non-magnetic material, in which μ $= μ_0$, the refractive index in defined by permittivity

$$n(\omega) = n_r(\omega) - in_i(\omega) = \sqrt{\frac{\varepsilon(\omega)}{\varepsilon_0}}.$$
(3.8)

Velocity (v) of the electromagnetic wave in the material depends on the refractive index

$$v = \frac{c}{n} \qquad\qquad\qquad (3.9)$$

3.2 Generation of electromagnetic waves

Electromagnetic (EM) radiation is generated when the unit of charge is accelerating. However, not all accelerating particles generate EM waves. For example, an electron circulating the atom nuclear generates no EM radiation even though it should do so according to classical electromagnetic theory. The quantum mechanical phenomena inhibit the radiation. However, the electron radiates due to motion between the energy states or orbits. When the electron "jumps" to the outer orbit e.g. due to external energy, and the state releases, the electron radiates electromagnetic radiation. There are some atom level phenomena which cause EM radiation such as nuclear magnetic resonance and electron-spin resonance.

EM radiation can be generated both naturally and artificially. Natural ways include, for example, radiation from flames, the sun, and space. In addition, electromagnetic radiation can be generated due to phenomena in the nuclei of the atoms. Gamma radiation is generated due to radioactive decay. Rontgen or X rays are generated more by external impactions, such as collisions by high energy (high speed) electrons with the nuclei of atoms. [Halliday, 1997].

All materials with a temperature over the absolute zero point 0 K, or -273.16 $^\circ$C, emit electromagnetic radiation. This radiation can be described by black-body radiation. Radiation due to a temperature rise can be seen a basis for background noise at micro and radio wave frequencies in the combustion chamber.

The spectral radiance B_v or radiation flux of electromagnetic radiation, as a function of absolute temperature T, is described by Plank's law.

$$B_v(T) = \frac{2hf^3}{c^2} \frac{1}{e^{\frac{hf}{kT}} - 1} \quad [\text{W/ (m}^2 \text{ sr Hz)}], \qquad\qquad (3.10)$$

where h is Planck's constant (6.63 $*10^{-34}$Js) and k is Boltzmann's constant (1.38*10-23 J/K). The function gives the emitted power per unit frequency, unit area of emitting surface and unit solid angle.

The radiance values were calculated as an example for furnace conditions at frequencies 1-21 GHz, a bandwidth of 1MHz and a temperature of 1000 $^\circ$C; see Figure 3.3.
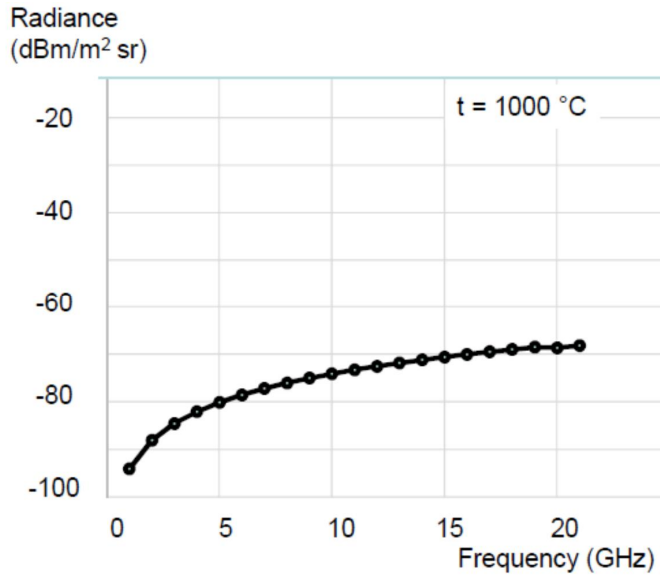
Radiance
(dBm/m² sr)

Figure 3.3: Radiance from 1 to 21 GHz at bandwidth 1 MHz and temperature 1000 ºC.

The radiance level, which can be seen as the background noise level, starts from level of about - 3 *10^{-10} mW/(m² sr) or -95 dBm/ (m² sr) at frequency about 1 GHz and reaches the value of about 1.52 *10^{-7} mW/ (m² sr) or -68 dBm/ (m² sr) at frequencies over 20 GHz.

The actual radiation from the surface of an object (a particle) depends on the *emissivity* of the surface. This describes how effectively an object radiates energy at a certain frequency compared to the black body. Emissivity e is defined as the brightness of an object at temperature T to the brightness of a black body at temperature T. [Woodhouse, 2006]

$$e = \frac{B_{f\_Greybody}}{B_{f\_Blackbody}}$$ (3.11)

The emissivity of flames depends mostly on the transparency or the thickness of the flames. For a thin layer of flames, the emissivity can be 0.48 or 0.72, depending on the measurement method. For thick layers of flames, as in large combustion chambers, the emissivity is near the black body emissivity or 0.9. [Agueda, 2010]

If the equation of black body radiation is integrated over the whole frequency band, we obtain total radiance (S)

$$S = \sigma T^4$$ (3.12)

The formula is known as the radiation law of Stephan-Boltzmann and σ is known as the Stephan-Boltzmann constant, ($5.6697 * 10^{-8}$ W/m^{2}K^4).

At the lowest end of the frequency bands or microwaves and radio waves under 300 GHz, where hf $<<$ kT, the Rayleigh-Jeans limit can be used. This reduces Planck's function to [Woodhouse, 2006]

$$B_v(T) \approx (\frac{2f^2k}{c^2})T \quad [\text{Wm}^{-2}\text{sr}^{-1}\text{Hz}^{-1}]. \tag{3.13}$$

This formula shows that the radiation is linearly related to the absolute temperature. From that, we can define the microwave brightness temperature T_B as

$$T_B(f) \approx \left(\frac{c^2}{2f^2K}\right)B_f = \left(\frac{\lambda^2}{2k}\right)B_f \quad [\text{K}]. \tag{3.14}$$

Related to microwaves, it is practical to speak of thermal radiation. The radiation is produced by thermal energy, which can impact at the electron or molecule levels. When the thermal energy is high enough, the electrons are knocked to upper energy levels and return back. These movements can be seen as changes in the positions and velocities of electrons or accelerations of charges. At slightly lower levels of heat energy, only molecule level vibrations and rotations take place, similarly causing radiation due to accelerations of charges packed in the molecules [Woodhouse, 2006].

Electromagnetic waves can be generated artificially. The process encounters in many ways depending on the frequency band. At radio and microwave frequencies, an electronic oscillator is used to generate alternating current, which is fed to an antenna. The antenna sends radiation and receives signals transmitted by other objects.

When an electromagnetic field is generated, three areas can be identified around the source (Figure 3.4): a reactive near-field, a radiating near-field and a far-field [Rahmat_Samii, 1997].
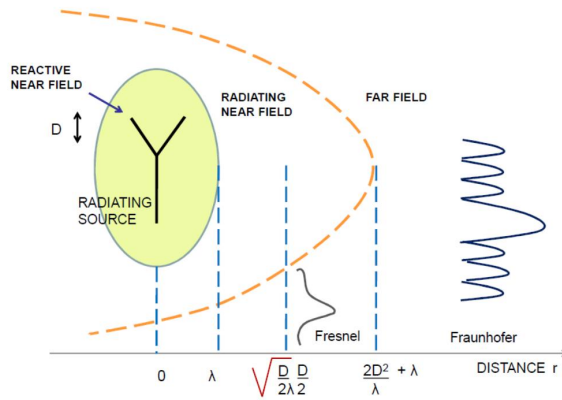
Figure 3.4: Fields around radiating source [Rahmat-Samii, 1995].

The boundaries of the fields are defined by the size (D) of the radiating object and wavelengths used. In the reactive near-field, the magnetic field dominates. The field supresses with factor $1/r^3$. In the radiating near-field, from distance $r > \lambda$, the magnetic field still dominates and the wave front starts to take shape. In the far-field, the electric and magnetic field propagate with the radial distance and field takes its final form. The field is decaying due to geometric dispersion and other attenuation mechanisms. In the far region, the real intrinsic impedance (Z_0) in free space conditions is

$$Z_0 = \sqrt{\frac{\mu_0}{\varepsilon_0}} = \mathbf{120}\,\pi \approx \mathbf{377}\,\Omega, \tag{3.15}$$

where μ_0 and ε_0 are permeability and permittivity, respectively, of the free space.

3.3   Propagation of radio and microwaves

The propagation of electromagnetic waves propagate as consecutive magnetic and electric fields. The antenna generates an alternating electric field, which produces an alternating magnetic field, and so forward. The propagation wave consists of electric and magnetic field pointers, which are contrary to each other and the direction of radiation. Also in the free space and lossy medium, this type of wave is called the transversal electromagnetic mode or wave (TEM); see Figure 3.5.
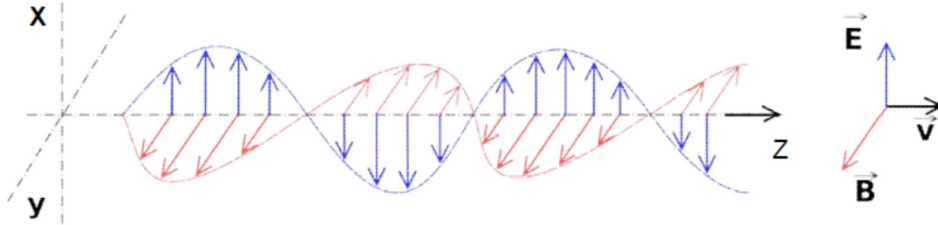
Figure 3.5: Electromagnetic TEM wave. E stands for electric field, B for magnetic field. The wave is propagating into the direction of z. Original picture [Lumen].

The time harmonic wave travelling in the far-field into the positive z direction can be described with wave equations unique to electric (E) and magnetic (B) fields based on Maxwell's equations

$$E_x = E_0 \, e^{-jkz} = E_0 \cos(\omega t - kz) \; ; \quad E_y = 0 ; \quad E_z = 0; \qquad (3.16)$$

$$B_x = 0 \; ; \; B_y = \frac{1}{\eta} E_0 e^{-jkz} = \frac{E_0}{c} \cos(\omega t - kz) ; \; B_z = 0 : \qquad (3.17)$$

where $c = \omega/k = 1/(\varepsilon_0 \mu_0)^{0.5}$ = speed of light in free space   (3.18)
             k = wave number and ω = angular frequency or 2πf.

In the equations, the term ωt stands for a momentary phase due to the angular speed and the term kz for the phase relating to a haul of signal from the starting point.

The relation between the electric and magnetic field of the propagation wave is called the intrinsic impedance or wave impedance (η) of the medium. It can be defined as

$$\eta = \frac{E}{H} = \sqrt{\frac{i\omega\mu}{\sigma + i\omega\varepsilon}} , \qquad (3.19)$$

where σ = conductivity (Ω).

The antenna structure defines the polarisation. It is defined by the direction of the electric field in the propagating wave. There exists linear polarisation, which is vertical or horizontal, and circular polarization, where the sum angles of electric and magnetic fields are rotating. The circular polarized signal is generated for example by a two-pole antenna, which is fed by two signals having a phase shift of 90 degrees.

Propagation and scattering of electromagnetic waves take place in many ways, depending on how the electromagnetic wave interacts with particles. If the frequency of the electromagnetic wave changes in collision, the scattering is called inelastic scattering, and in other cases, elastic scattering. In radio and microwaves, the frequency does not change

in scattering. That is why all scattering at those wavelengths is elastic. Figure 3.6 displays the detached propagation of radio and microwaves in a free space, a lossy medium, conductors and plasma.

ωp > ω — REJECT

(WEAK) PLASMA

ωp < ω — LINEAR or BENDING PROPAGATION

FREE SPACE

$v = vo$

SPREADING WITHOUT REFLECTIONS

ATTENUATION $S = f(1/R^2)$

CONTINUOUS PHASE ROTATION

SPREADING WITH REFLECTIONS FROM OBJECTS

TUNNELING $S = f(1/R^n)$

FADING $S = f(t)$

STEP-WISE PHASE CHANGES

PHASE CHANGE

REFRACTION $v = f(\sin\theta)$

PROPAGATION OF RADIO AND MICROWAVES

SCATTERING

DIFFRACTION

REFLECTION <   TUNNELING / FADING

LOSSY MEDIUM

$v < vo$

ABSORPTION

DIFFUSE REFLECTION

ATTENUATION $S = f(e^{z\alpha})$

CONDUCTORS

$v < vo$

OVER CROSS SECTION

ON THE SURFACE LAYER

SKIN DEPTH

WAVE GUIDE

PHASE CHANGE (IMPEDANCE)

ATTENUATION (IMPEDANCE)

v = velocity of signal
vo = velocity in free speed
ω = angular speed of signal = $2\pi f$

Figure 3.6. Radio and microwaves propagate and scatter in a free space, a lossy medium, conductors and (weak) plasma in different ways. *vo* stands for signal velocity in the free space, *v* for actual velocity in the medium, ω for the angular speed of the signal and ωp for the angular speed of the plasma or plasma frequency ($\omega_p = 2\pi f_p$).

In the following, the attenuation and mechanisms are studied for the free space, lossy medium and plasma cases. Plasma is also taken under consideration based on many research results stating that at least weak plasma exists in combustors. Plasma conditions prevail if the amount of free charges, in practise electrons, is more than $10^{10} – 10^{12}$ /cm^3. [Mphale, 2008]. Weak plasma conditions, prevailing e.g. in an ionosphere, contain more than $10^2 – 10^6$ electrons/cm^3 [Aikio, 2011]. The presented limits differ slightly depending on the source. Plasma conditions have a great impact on radio and microwave propagation [Fitzpatrick, 2013].

3.3.1 Attenuation in free space

When a radio signal propagates in a free space, the signal is attenuated in several ways: due to (geometric) spreading, due to reflections causing summing of signal of different phases, and due to polarization.

The attenuation due to spreading takes place according to the Friis law, which defines the signal spreading as a function of the second order of distance and wavelength of the signal. The law describes the relation of received power of signal to transmitted power of the signal

$$\frac{P_R}{P_T} = G_t G_R \left(\frac{\lambda}{4\pi D}\right)^2$$

(3.20)

where

P_R = received power in the antenna output port without internal dissipations of antennae (W), P_T = transmitted power in the antenna port without internal dissipations of antennae (W), G_t = the gain (~ directivity) of the transmitter antenna, G_r = the gain (~ directivity) of the receiver antenna, λ = wavelength (m) and D = distance between the transmitter and receiver antennae (m).

The formula is typically written in a more practical form of a link budget (3.21)

$$\Delta P = P_T - P_R = G_T + G_R + 20\,log\left(\frac{\lambda}{4\pi D}\right) - G_s.$$

(3.21)

All parameters are given in decibels (dB). P_R is the lowest possible received power for adequate signal-to-noise ratio (SNR) for receiving. ΔP is link attenuation. The typical allowed link attenuation or path loss, depending strongly on the system, is from 90 to 130 dB, and in special cases, much more [Hernando 1999; Braasch, 1999]. G_s describes the so-called system gain, which means signal processing, e.g. coding or other digital handling, which is used to improve signal quality for receiving and decoding.

The combustion chambers are closed spaces with walls of metals, typically iron compounds, and stone or cement materials as bricks or casted. The propagation of the radio and microwave signal is affected by several mechanisms related to the walls and other objects inside the combustion chamber. These mechanisms are reflection, diffraction, refraction and scattering; Figure 3.6 and Figure 3.7.
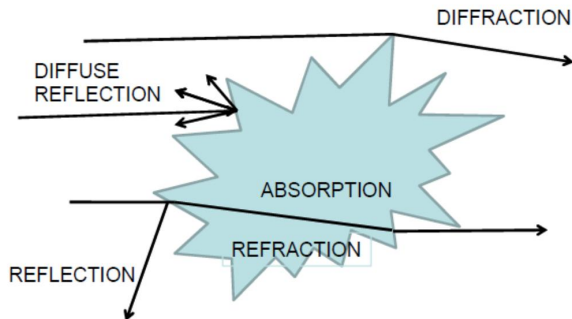
Figure 3.7: Diffraction, reflection, refraction and absorption of EM wave in collision with an object.

Reflection occurs when radio or microwave or generally the EM wave falls on an object having large dimensions compared to the wavelength. If the wave falls to a dielectric surface, part of it is reflected back and part is transmitted or absorbed. The reflection is dependent on the angle of the incident wave direction (wave vector) and the normal of the surface (θ). If the diffraction factors are different in the mediums, the signal will be refracted or the angle of the propagating wave will be different to the incident angle. If the wave falls on a metallic surface, all wave energy is reflected back. The reflection of energy also depends on the polarization of the wave.

Diffuse reflection is a consequence of reflections from a coarse surface. Each unique mode of a wave will reflect uniquely depending on the angle of incident to the surface normal.

Reflections pose great challenges to communication due to interferences of sent and reflected waves. In the interferences, signals propagate different paths and path lengths. Different paths cause a phase difference between partial signals. When partial signals of different phases are summed, the signal can be attenuated and will increase in power. This means that the strengths of signals propagating between objects are experienced varyingly and phases of signal components fluctuate. This phenomenon is called multi-path attenuation or fading. The variations in strengths of sum signals can be tens of decibels.

Electromagnetic wave can travel behind an object due to phenomenon diffraction. The phenomenon is described as Huygen's principle [Halliday, 1997]. According to it, every point of a wave front acts as a new source of radiation, producing wavelets which according to the time of arrival are delayed, and when combined, form a new propagation wave front.

3.3.2   Attenuation due to polarization

Polarization means the direction of the electric field vector in a free space. There are linear polarizations, such as horizontal and vertical polarization, and cross polarization. In cross polarization, the field vectors are circulation to the right (right hand circular polarized or RHCP) and to the left (left hand circular polarized or LHCP). The polarization of a transmitted signal is initially defined by the antenna structure and signal feed. Attenuation due to polarization is meaningful especially at short distances, or when the reflection and other multipath effects have not mixed the intrinsic polarization. The polarization loss can be calculated as [Radicella, 2004;]

$$A_P = 20 \lg(\cos \phi),$$
(3.22)

where A_P is the propagation loss due to mismatched antenna polarization planes, and ϕ is misalignment angle between two antennas. Table 3.1 shows calculated values for losses due to polarization.

Table 3.1: Attenuation in decibels (dB) due to polarization mismatch between transmitter and receiver antenna.

	Vertical	Horizontal	LHCP	RHCP
Vertical	0	-20	-3	-3
Horizontal	-20	0	-3	-3
LHCP	-3	-3	0	-20
RHCP	-3	-3	-20	0

In the table, attenuations of -20 dB are practical values, but theoretically attenuation is infinite. Although many factors, such as multipath propagation, reduce the effects of polarization on attenuation, a polarization mismatch can significantly weaken transmission especially in open areas.

3.3.3   Attenuation in a lossy medium

A medium is called a lossy medium or lossy dielectrics, if EM wave loses power as it propagates in the medium. The power loss is the greater the better the conductivity of the material (σ) is. Conductivity is calculated related to the frequency as in equation (3.23)

$$\sigma \;=\; \omega\epsilon'', \tag{3.23}$$

in which ε'' is the factor of the imaginary part of permittivity given in equation 3.7. When the radio or microwaves propagate in the z direction in the lossy medium, the signal is attenuated exponentially, or

$$E \;=\; E_0 \cos(\omega t - kz) * e^{j\gamma z} \tag{3.24}$$

or otherwise written as

$$E \;=\; E_0\, e^{-\alpha z} \cos(\omega t - \beta z). \tag{3.25}$$

In eq. 3.24, γ is a complex attenuation factor

$$\gamma \;=\; \sqrt{i\omega\mu(\sigma + i\omega\varepsilon)} \;=\; \alpha + i\beta \tag{3.26}$$

For α and β in low-loss dielectric material or lossy material, in which

$$\frac{\sigma}{\omega\epsilon_r} \ll 1 \tag{3.27}$$

where

ε_r = real part of complex permittivity.

The following approximations can be given [Hui, 9]:

$$\alpha \;=\; \frac{\omega e_i}{2}\sqrt{\frac{\mu}{\epsilon_r}} \qquad\qquad \text{[Np/m]} \tag{3.28}$$

$$\beta \;=\; \omega\sqrt{\mu\epsilon_r}\left[1 + \frac{1}{8}\left(\frac{\epsilon_i}{\epsilon_r}\right)^2\right] \quad \text{[rad/m]}. \tag{3.29}$$

The attenuation is due to the incomplete polarization of dielectric particles in which process the radio and microwave losses energy. At radio and microwave frequencies, the quantum of radiation (E = hf) is so small that no electron orbit changes can take place. Therefore, the power loss changes to the thermal energy of molecules, not to radiation.

3.3.4   Measured attenuation values in a lossy medium

To obtain practical values for attenuations in a lossy medium, some papers considering the effects of sand in different forms on attenuation were studied. Most examples deal with measurements in sand storms. The effects of sand storms in Iraq have been studied e.g. by Abdulla [1988]. During storms, particle diameters vary from 1.4 to 6.9 μm. The attenuation result was given for frequency band from 0.5 to 37 GHz. The moisture of sand

strongly affected the results. At a moisture level of 0.3 %, the attenuation was 0.08 dB/km at a frequency of 37 GHz, and at a moisture level of 10%, the value was about 0.7 dB/km at the same frequency. Unfortunately, Abdulla does not specify the densities of the sand in the air. Abuhdima and colleagues bind the attenuation to relative visibility in their studies. They suggest an attenuation of about 0.7 to 0.8 dB/km in low visibility at frequencies 15 GHz and 20 GHz, respectively. In addition, they have measured an attenuation of 0.241 dB/km at 2.54 g/m^3. [Abuhdima, 2010] Also Vishvakarma et al. have bound attenuation to visibility. The greatest attenuation they suggest is about 100 dB/km at a frequency of 70 GHz and a particle size of 1 mm.[Vishvakarma, 1981]

Williams and Greeley have studied the attenuation of sand layers on microwaves. Again, the moisture plays a significant role in attenuation. Attenuation due to sand with a moisture level of 0.3 % varies from 2.0 to 5.9 $\pm$ dB/m at frequencies from 0.5 to 9.6 GHz. At a moisture level of about 10.7 %, the attenuation varies from 5.0 to 323.3 dB/m [Williams, 2001].

4   Radio and microwaves in flames and combustors

Attenuation and noise are the main issues to be studied when applying radio and microwaves in flames and combustion chambers. This chapter introduces attenuation and noise issues from a practical perspective. All attenuation mechanisms introduced earlier in sections 3.3.1, 3.3.2 and 3.3.3 are relevant in flames and combustors. For free path loss calculations, the noise and signal-to-noise ratio must be taken into account. Moreover, additional attenuation will result from suspensions and ionization in high density areas. In fact, the latter seems to be the most important mechanism of attenuation at low frequencies in strongly ionized flames and combustion environments. This section later introduces other mechanisms, such as attenuation due to refraction and multipath effects in the combustion chamber.

It is important that the dimensions of a small combustor are appropriate for the wavelengths of signals used. To guarantee far-field conditions and reliable results from equation (3.20), it is recommended that the minimum dimensions in a chamber are about ten times the wavelength of the signals. The path loss and available operation margin calculated by the link budget (3.21) increase more notably when the noise present in combustion chambers reduces the basic sensitivity of operating wireless devices.

Microwaves are quite seldom applied to real combustion processes. However, researchers have carried out some practical tests. The most common and perhaps beneficial application is the use of microwaves to reconditioning coal for combustion, making coke and taking measurements, such as mass flow and flow velocity measurements [Binner, 2014; Blankinship, 2004; Lipták, 2017]. Some measurement applications have been employed in very high temperature flames and in laboratories [Stockman, 2009; Rao, 2011]. Stephan et al. [2004] have developed temperature sensing based on microwave radiation. Hauschild and Knöckel have used microwaves for measuring density profiles in fluidized bed reactors. They have created a development method for better spatial resolution based on a spatial location reflectometer. The method operates only at short distances, and practical tests described in the paper have been performed in a laboratory environment. [Hauschild, 1995] They give no exact values for attenuations, only for relative permittivity.

4.1   Attenuation in flames

No free electrons and charged atoms exist in flames due to chemical and thermal ionization. Ion concentrations cannot be very precisely determined. According to investigations, ionization in free burning hydrocarbon flames can be about $4.3*10^{10}$

ions/cm^3 and in acetylene flames $7*10^9$ ions/cm^3 [Mphale, 2006]. For pine needles in flames, the electron density is $1.32*10^{10}$/cm^3 [Mphale, 2007-2].

Thermal ionization happens when electrons are thermally excited to free electrons from materials in flames. Thermal ionization is strongly dependent on the temperature and typically takes place in materials having low ionization potential or activation energy. Such materials are alkalines, such as potassium (K) and sodium (Na) compounds. Their first ionisation potentials are 4.318 eV and 5.2 eV, respectively. Other materials with low ionisation potential are e.g. calcium (Ca, 6.09 eV), magnesium (Mg, 7.61), and silicon (Si, 8.12 eV). [Heron, 2004]

Chemi-ionization is another mechanism for ionization. Typically, chemi-ionization occurs as hydrocarbon chemical reactions. It takes the required energy from dissociation energies released in the dissociation of materials in exothermic chemical reactions. It partly takes energy from flames.

Electrons are about 2000 times lighter than the unique (charged) nuclei of atoms. Consequently, electrons have a greater impact on the propagation of an electromagnetic signal. Electrons are accelerated in a microwave or electromagnetic field, absorbing energy from the field. Electrons loose energy through collisions and cause the attenuation of electromagnetic waves. The more free electrons (and ions) there are, the more collisions there are and the greater the attenuation of the signal is.

In equation (3.25), α and β describe the attenuation and phase shift, respectively. They can be defined through permittivity, permeability, conductance and angular speed [Green, 1964]:

$$\alpha = \omega \sqrt{\frac{\mu\varepsilon}{2}\left[\sqrt{1 + \left(\frac{\sigma}{\varepsilon\omega}\right)^2} - 1\right]} \qquad \text{[Np/m]} \tag{4.1}$$

$$\beta = \omega \sqrt{\frac{\mu\varepsilon}{2}\left[\sqrt{1 + \left(\frac{\sigma}{\varepsilon\omega}\right)^2} + 1\right]} \qquad \text{[rad/m]} . \tag{4.2}$$

In calculating the propagation factors α and β in flames, the concept of plasma frequency must introduced. It is the characteristic frequency of collective electron oscillations in the plasma. The plasma frequency is mostly dependent on the electrons because, as mentioned above, electrons have a greater mobility and oscillation capability.

The plasma angular frequency (ω_p) is calculated as follows:

$$\omega_p = \sqrt{\frac{n_e e^2}{m_e \varepsilon_0}} \; , \tag{4.3}$$

where n_e is the electron count, e the charge of an electron, m_e the mass of an electron, and ε_0 the permittivity of the free space or vacuum. The following example gives an idea of the order of the plasma frequencies: The electron density of a pine litter flame could be $1.35 * 10^{10}$ electron/cm^3 [Mphale, 2007-2]. According to equation (4.3), the angular plasma frequency is $6.55*10^9$ rad/s $\approx 1,04*10^9$ Hz or 1,04 GHz.

The attenuation factors α and β are defined in bushfires and experimental firing tests when illuminated by electromagnetic waves as follows [Letsholathebe, 2015; Mphale, 2008]:

$$\alpha = \frac{\varphi_{eff}}{2c}\left[\frac{\omega_p^2}{(\omega^2 + \varphi_{eff}^2)}\right] \qquad (4.4)$$

$$\beta = \frac{\omega}{c}\left[1 + \frac{\omega_p^4}{8(\omega^2 + \varphi_{eff}^2)^2} \cdot \frac{\varphi_{eff}^2}{\omega^2}\right], \qquad (4.5)$$

where φ_{eff} is the electron-neutral collision frequency and ω the angular frequency of the electromagnetic signal.

Green suggests the calculation of α and β through the plasma frequency by the following approximations [Green, 1964]:

$$\alpha \approx \frac{\omega}{c}\left(\frac{\left(\frac{\omega_p}{\omega}\right)^2 \frac{\varphi_{eff}}{\omega}}{\left[1 - \left(\frac{\omega_p}{\omega}\right)^2\right]^{1/2}}\right) \qquad (4.6)$$

$$\beta = \frac{\omega}{c}\left(\frac{1}{\left[1 - \left(\frac{\omega_p}{\omega}\right)^2\right]^{\frac{1}{2}}}\right). \qquad (4.7)$$

In equation (4.7), we see that when the signal frequency ω is less than the plasma frequency ω_p, the nominator becomes imaginary. This is interpreted so that the signal does not propagate at frequencies lower than the plasma frequency. On the contrary, they refract or reflect.

For the momentum transfer collision frequency φ_{eff}, papers offer many solutions. Letsholathebe and colleagues have collected examples of solutions [Letsholathebe et al., 2014]. Boan gives examples of the collision frequency in different types of flames; see Table 4.1.

Table 4.1: Examples of flame collision frequencies [Boan, 2009]

Conditions	φ_{eff}
Acetylene – air 760 mm Hg, 2480 K	$2.6 * 10^{11}$
Acetylene-Oxygen 7.7 mm Hg, 2300 K	$3.7 * 10^9$
Coalgas – air 760 mm Hg, 2200 K	$8.8 * 10^{10}$
Pine needles – 1013.25 hPa, ~1100 K	$3.43 – 5.97 * 10^{10}$

Practical values for attenuation have been collected in many practical measurements in forest fires and small-scale laboratory combustion assemblies. Mphale and his colleagues have done research work for clarifying the attenuation mechanisms and for practical values of attenuation and phase shifts. According to the investigations of his research group, in forest fires, part of the signal between communicating units is reflected (up), but most of it is clearly attenuated. At VHF or frequencies from 300 to 800 MHz, at temperatures from 950 to 1150 K, the attenuation in grass fires ranges from 0.001 to 0.49 dB/m. At a potassium content of 0.5 %, the attenuation ranges from 0.007 to 0.24 dB/m. [Mphale, 2006-2].

With flames burning the dried forest fuel for ten days, the attenuation ranged at a frequency band of 10–12.5 GHz from 9 dB/m to about 6 dB/m with eucalyptus litter, from 7 dB/m to about 4.8 dB/m with grass, and from 4 dB/m to about 3 dB/m with pine litter. The results were measured at temperatures of 730-1000 K. [Mphale, 2008] At higher frequencies from 30–60 GHz and a temperature of 1000 K, the attenuation in shrub fires ranged from 0.06 to 0.7 dB/m. However, with a higher temperature of 1150 K and an increased potassium content (1 %), the attenuation increased to a range of 7.44 – 24 dB/m [Mphale, 2007-3].

Phase shift issues are excluded from this thesis because they are meaningful only at short distances between measured points or in a laboratory. In combustion chambers, phase shifts are more inaccurate due to reflections and large dimensions.

4.1.1 Attenuation in kraft recovery boiler

As stated earlier in the thesis, the attenuation of radio and microwaves in flames depends on the charged particles, especially electron concentrations in the flames. In addition, in this thesis has presented practical measured values for radio and microwave attenuation in forests, forest litter or bush fires. Some values are also given in [Korhonen, 2017-4].

To understand microwave attenuation inside a combustion chamber, practical measurements were performed in a kraft recovery boiler. The boiler is part of the pulp and paper mills in Varkaus, Finland, owned by Stora Enso Ltd. The boiler was built in 1970 by Ahlstrom Machinery Ltd. It is designed to produce 33.8 kg/s of steam at a pressure of 60 bar and a temperature of 475 ºC, offering thermal energy at a capacity of about 114 MW. The fuel of the boiler is black liquor. In addition, oil is used as support in start-ups and shutdowns. The black liquor consumption varies from 935 to 1150 tons ds per day, calculated at a 72 wt% dry solid content. The dimensions of the combustion chamber are a height of about 28 meters and a bottom area of approximately 60 m^2.

Practical attenuation tests were made through the boiler, from one spraying port opening (Figure 4.8) to another on the opposite wall. The measurements were done at frequencies of 2-18 GHz. The measurement equipment included two broadband directional antennas, type LB-20180 (A-Info Ltd.), Figure 4.1, and a vector network analyser (VNA) type E5071C, option 2K5, manufactured by Agilent Technologies Ltd., Figure 4.2. The antennas were connected to the VNA with coaxial cables. The bandwidth of the VNA was 20 GHz. The antennas' frequency band was 2-18 GHz. The IF bandwidth of the VNA was set to 10 Hz to maximize the device's system performance.

Figure 4.1: Horn antenna LB-20180 at sprayer port of a kraft recovery boiler for attenuation and noise measurements.

Figure 4.2: Vector network analyser (VNA) in measurements at kraft recovery boiler.

The measurements were carried out in the operational boiler. The boiler was operating at a reduced output – only three of four possible black liquor sprayers were in use. The reference values were measured in an open area (yard), and in a cold boiler. Further, there was no EMC chamber available for the reference measurements. Figure 4.3 shows the measured attenuations.
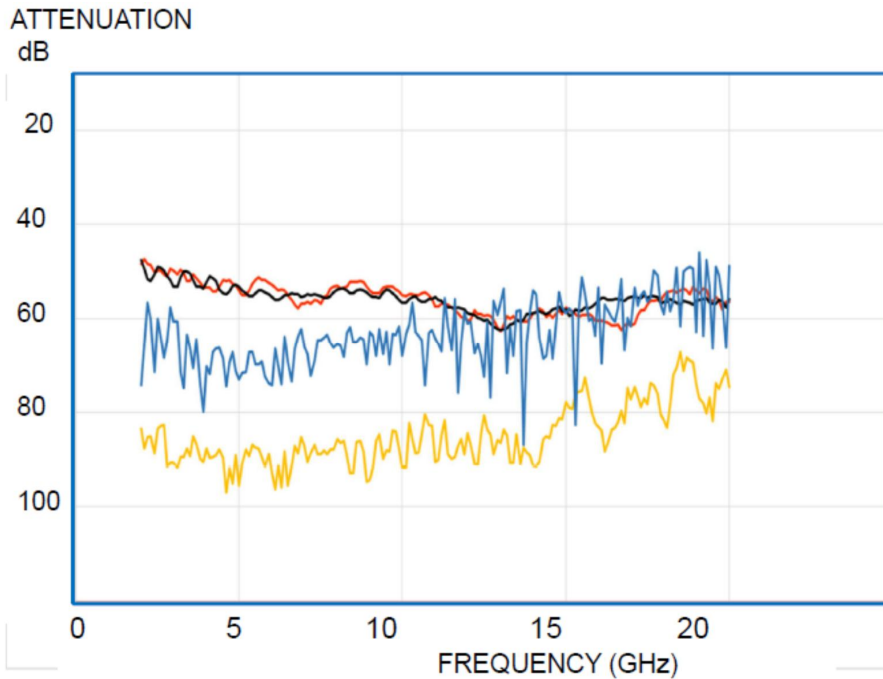
Figure 4.3: Microwave attenuation in kraft recovery boiler at frequencies 2-20 GHz. Curves, see text.

   In Figure 4.3, the red curve describes the attenuation between antennas in a free space (yard). The black curve is rather the same shape, excluding the highest frequencies, with the described attenuation when antennas in the free space are equipped with plated tunnels simulating the port structure (see Figure 4.4). The blue curve describes attenuation through a cold boiler, and finally, the orange curve describes the attenuation through an operational boiler or effects of the flames and ionization. The blue curve is taken from another data set. It was measured with an IF bandwidth of 70 kHz, which is the default bandwidth of the VNA. The curve is adjusted to levels that are10 dB lower to compensate for the wider bandwidth compared to other curves.

   When looking the curves, the conclusion can be drawn that all curves tend to show smaller attenuation at higher frequencies. This phenomenon can be best depicted by antenna gains, although they were principally compensated for in the calculations. The attenuation tends to decrease especially at higher frequencies in the cold boiler. This phenomenon obviously originates from chamber effects of a closed space; metallic walls reflect signals, adding power compared to the direct signal between the antennas. The attenuation due to flames and ionization (orange curve) decreases quite strongly at the highest frequencies, having remarkable variations. The behavior of this curve can partly be described as above, but there is still a suspicion of the effects originating from indefinitely unaccountable phenomena. The final conclusion is that the attenuation of flames and ionization through this KRB is on average about 90 dB, 90/8.8 dB/m or about 10 dB/m.

Figure 4.4: Testing microwave attenuation behaviour through spraying port models at the yard. The antenna is in back position in the left figure.

4.1.2   Attenuation due to suspensions in combustion chamber

Attenuation due to suspensions mainly concerns CFB boilers and lower parts of BFB boilers. The attenuation due to suspension and particles in combustion chambers, where municipal waste is burned, is unclear at the moment of writing this thesis. The issue requires further investigation.

4.1.3   Attenuation without media attenuation in combustion chamber

This section ignores the attenuation due to a lossy medium and examines the attenuation due to a phenomenon called fading, where the signal attenuates and the signal frequency fluctuates due to reflected and interfacing signals originating from the signal itself. [Hernando, 1999]

The walls of combustion chambers are made of iron and concrete compounds. Metallic surfaces radiate practically all of the radiation falling on them. Wall parts made from concrete compounds reflect the majority of the signal; the rest is transmitted in the material. Consequently, in combustors with low attenuation (if ever possible), signals will

reflect and fade in many ways. In practice, the tube walls of combustion chambers cause strong diffuse reflections of the signals. (Figure 4.5)
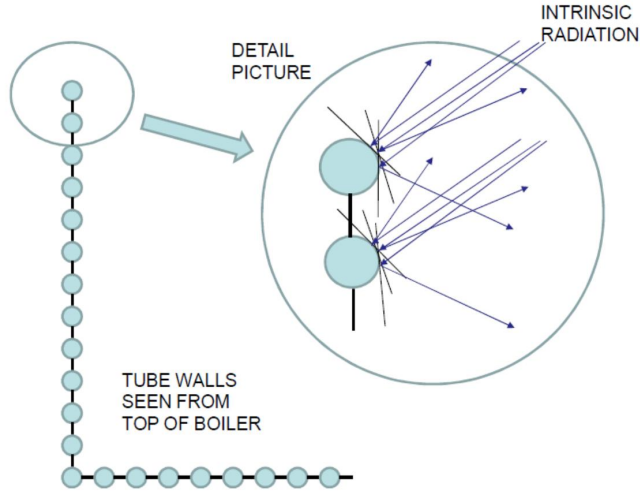

Figure 4.5: Diffuse reflections from surfaces of tube walls and exchangers

Reflections cause multipath propagation and consequently strong fading in a mobile sensor travelling in the combustion area. In digital communication, signal strengths can vary from twice the original signal down to zero level due to fading [Hernando, 1999; Watteyne, 2010]. In the form of an equation, the multipath fading from N arbitrary directions is [Hernando, 1999]

$$ e_r = \sum_{i=1}^{N} e_i e^{i2\pi f_t t} e^{j\frac{2\pi}{\lambda} v t cos\theta_i} , \qquad\qquad (4.8) $$

where e_r is the received summarized signal, N is the arbitrary interfacing signal count at the receiver port (antenna), f_t is the frequency of the original or transmitted signal, t is time, v is the velocity of signals, and θ_i is the reflection phase of each unique signal. The equation demonstrates both the frequency shift (Doppler phenomena) and amplitude fluctuations.

4.1.4 Refraction in combustion chamber

Sinusoidal electromagnetic waves cannot propagate through plasma if the frequency of the signal is lower than plasma frequency [Ransom, 2016]. Further, the plasma reflects or refracts such signals. The waves propagating through (un-magnetized) plasma seem to

disperse or refract in different ways depending on the frequency because the refractive index depends on the frequency. This can be expressed as follows [Ransom, 2016; Fitzpatrick, 2013]:

$$n = \frac{k\,c}{\omega} = \sqrt{1 - \frac{\omega_p^2}{\omega^2}} \; , \qquad\qquad (4.9)$$

where k is the wave number, c the velocity of light in a free space, ω_p the angular plasma frequency, and ω the angular frequency of the electromagnetic signal. A practical example of it is e.g. the behaviour of radio and microwaves in the ionosphere: the low frequency signals, such as HF and VHF radio signals, refract from the ionized ionosphere while the high frequency signals go through directly, such as in satellite communication. [Ransom, 2016]

The refraction can attenuate the signal transmitted from a point in the combustion chamber. This occurs when the combustion has hot points, typically in the middle of the boiler. The refractive index decreases with an increasing temperature [Boan, 2009]. Consequently, the signal tends to refract in lossy material from an area of a low refractive index into the direction of a higher refractive; see Figure 4.6.
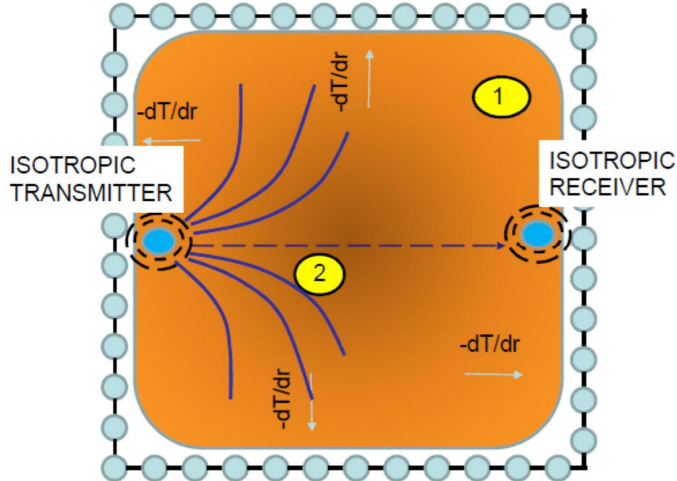

Figure 4.6: The refractive index tends to increase from the middle to the sides of the combustion chamber. This may increase attenuation in some parts of the chamber and in direct-through measurement (dashed line). The darkest colour indicates the highest temperature.

The above-mentioned phenomenon complicates the measurement of attenuation directly through the boiler (dashed line) from transmitter to receiver (antenna) because part of the signal power can be redirected from the centreline to the sides of the boiler (blue lines in Figure 4.6.) In conclusion, the field strength varies from one position to another inside the chamber. For example, as graphically represented, sensor ball number 1 could be in a considerably better field than sensor ball 2.

4.2   Noise in combustion chamber

As pointed out earlier in this thesis, noise is comparable to the absolute temperature and bandwidth. High temperatures in combustion chambers raise the noise level from that experienced in normal conditions. Consequently, noise must be taken in account when designing devices communicating or measuring at radio and microwave frequencies or with electromagnetic waves in general.

Noise impacts the receiving of radio and microwave signals; see Figure 4.7. The normal operation situation is described on the left. The background noise is at a low level. It is lower than basic sensitivity of receiver, on which adequate SNR relative to data speed is reached. Adding to that attenuation from the link, the transmission of power is defined according to equation 3.20. In the middle of Figure 4.7, the base floor noise has risen. In this case, the transmission level must be increased to achieve a sufficient SNR. On the right, the noise is very high e.g. due to the high temperature and/or wide bandwidth. The situation is non-operational because the attenuation of the link is fixed and the transmitter is sending at a maximum power level. The noise exceeds the sensitivity of the receiver. In some cases, the situation can be corrected by signal coding. For example, in a GPS system the signal received by land objects is under the noise level and can be decoded only by predetermined codes used in GPS data. This type of coding in the communication of wireless sensors is not available without special arrangements. In addition, coding increases the required bandwidth.
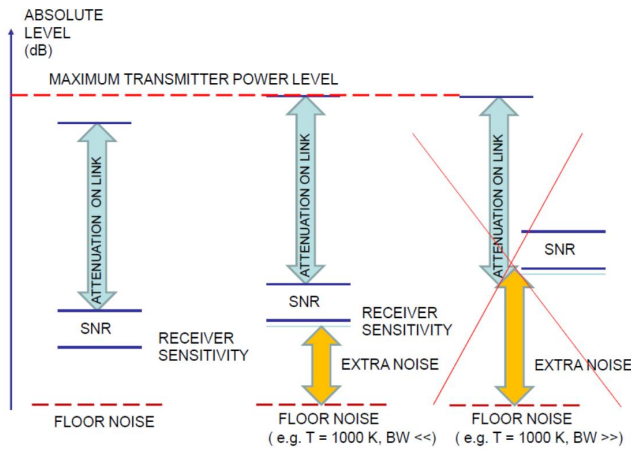
Figure 4.7: Relation between noise, sensitivity, SNR and transmission level.

4.2.1   Noise in kraft recovery boiler

The noise, discussed initially in section 3.2, in the kraft recovery boiler was measured and some conclusions drawn considering the noise levels and bandwidths. The issue is elaborated on in [Korhonen, 2017-1]. In the measurements, noise was measured during full boiler operation at a frequency band of 2-19 GHz from the sprayer port of the boiler. In addition, the temperature was measured with a FLIR T200 IR thermal imaging camera. Figure 4.8 shows the temperature profile in flames through the sprayer port.
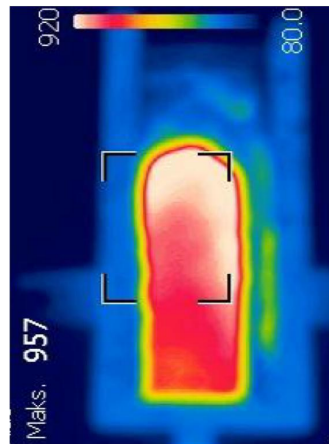

Figure 4.8: View of IR camera from spraying port of a KRB. The highest temperature is about 957 ºC.

The temperature measurements employed the emission factor 1. The highest temperatures according to the IR photo are of the order of 950 ºC.

The noise level measurements were conducted with the spectrum analyser MS2720T of Anritsu Company Inc. The analyser has a bandwidth from 0 to 20 GHz and its base floor noise is about -160 dBm/Hz with a 20 dB internal preamplifier. LB-20180 Broadband horn antennae manufactured by A-INFO Ltd. were used. The operating frequency band of the antennae was 2–18 GHz (S_{11}<-10 dB).

Figure 4.9 shows a noise level over the whole band with video and resolution bandwidths of 1 kHz as an example.
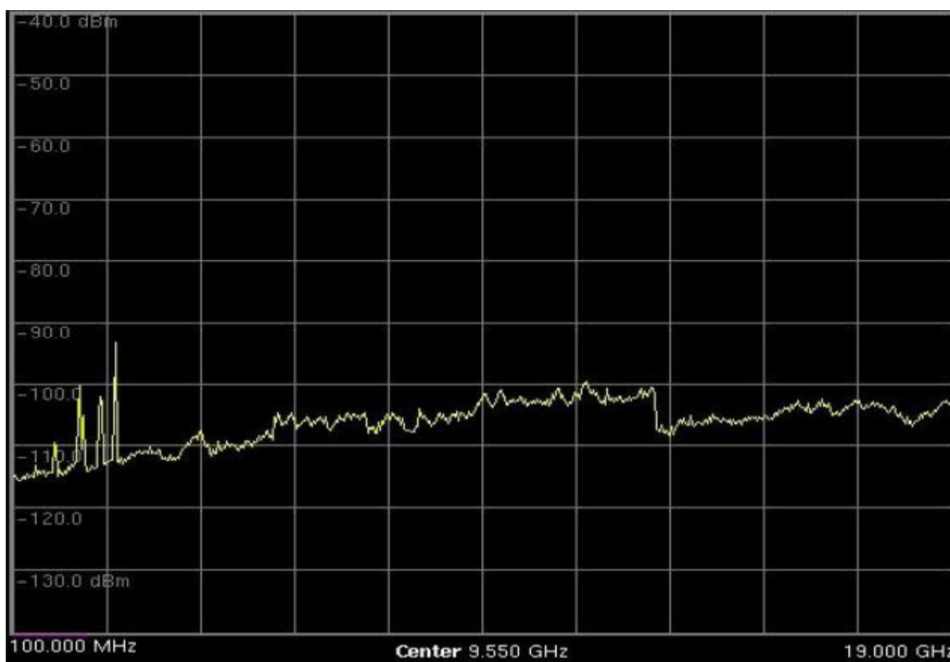

Figure 4.9: Noise level in a KRB at frequencies 0.1-19 GHz, RBW=1 kHz, VBW=1 kHz.

In the figure, only frequencies of 2 GHz or higher are relevant because the antenna gain was defined only from the operation frequency of 2 GHz. However, in the lowest frequency area, signals from the mobile network base station and WLAN station can easily be identified. Compared to Figure 3.1, taking the smaller bandwidth into account (meaning a reduction of 30 dB), the noise level of about -110 dBm is 20-30 dB higher than the noise level outside the combustion chamber at those frequencies. At higher frequencies, the noise level difference evens out. At the highest frequencies, the noise level is roughly the same level as outside the combustion chamber.

Noise levels in the KRB environment seem to rise especially at large bandwidths to levels which clearly limit applying wideband wireless techniques, such as Bluetooth and WLAN, in those environments. [Korhonen, 2017-1].

5   Operation time of a sensor in a combustion environment

In this chapter operation or lifetime of the sensor in combustion area is studied. The operation time of normal electronics in flames is very short, and high temperature electronics is still under development. The operation time of the sensor is extended by a protective cover made from fire-tolerant materials. These materials are studied and operation times are modelled and simulated and tested in real flame environment. The material is partly the same in [Korhonen, 2017-3].

The operation time of a sensor operating at a high temperature depends on many factors. The main limiting factor is the operation temperature of electronics in the sensor. As stated later in this thesis, electronics devices which tolerate temperatures as high as in combustion chambers and which have sufficient operational capabilities for an active sensor are not available commercially. Consequently, it is more functional and even necessary to use electronics intended for normal temperatures and to protect it with an enclosure. Furthermore, it must be accepted that the operation time of sensor electronics is limited, and without special arrangements, it will be short due to the rising temperature in an enclosure. The increase in temperature depends on self-heating due to the power dissipation of the electronics and heat flow from the environment surrounding the enclosure. There are means to extend the operation time. In this section, operation time issues are studied, focusing on passive thermal protection or insulation. All active cooling methods are excluded from the study.

5.1   Application of electronics at high temperatures

Researchers have studied high-temperature electronic sensors for quite a long time [Turner, 1994]. The research has mainly focused on surface acoustic wave (SAW) sensors. Hornsteir [1998] investigated SAW sensors and their materials based on lithium, langasite and aluminium nitrides. He has concluded that e.g. $LiNbO_3$ is suitable for long-term operation at 300 ºC, but tolerates 800 ºC only a short time. In addition, gallium lantanium silicate or LGS ($La_3Ga_sSiO_{14}$) can principally operate at 1470 ºC because of its steady phase action. However, the material has some other properties making it difficult for sensors. Hornsteir's conclusion was that SAW devices can be applied at temperatures up to approximately 1000 ºC, if appropriate material combinations are used. Mrosk [2001] has studied material issues related to sensors and maintains that due to the melting of aluminium at quite low temperatures (660.3 ºC), aluminium is not a suitable material for a SAW sensor reflector. Therefore, platinum must be used in the reflectors. Mrosk states that monocrystalline LGS or langasite ($La_3Ga_sSiO_{14}$) can lose piezoelectric properties at 1000 ºC [Mrosk, 2001]. According to another study, both temperature monitoring and identification is possible at up to 400 ºC [Hauser, 2005]. Many papers [e.g. Fachberger, 2006] concentrate on temperature measurements using SAW sensing technology. Some research papers focus on special SAW sensor investigations, such as

gas sensors [Zeng, 2011; Thiele, 2005], pressure sensors [Moulzof, 2010] and strain sensors [Shu, 2015].

SAW-based sensors are developing quite quickly. However, challenges in applying SAW sensors to process parameter monitoring in industrial combustion chambers are still quite significant. Because the positioning of RFID or SAW tags is challenging in normal environments [Bouet, 2008], obviously it would be extremely difficult to position mobile SAW sensors in a combustion area. The fluctuating signal attenuation and propagation velocity inside a combustion chamber make ordinary small-scale time and signal strength based positioning systems worthless, see section 7.2. In summary, the use of SAW sensors is and will for the foreseeable future be limited in high-temperature mobile sensor applications.

5.2   Operation time inside thermal insulation

To extend operation time of an ordinary electronics inside sensor ball, the cover of sensor ball must function as thermal protection, which decreases heat flow from the combustion environment flowing inside the sensor ball. Decreasing heat flow delays the warming of the sensor and thus stretches the operation time. In tandem, the external flow is minimized and self-heating must remain low enough to hinder excessive warming of the sensor electronics. In its entirety, the operation time is a compromise of many contradictory issues; see Figure 5.1.
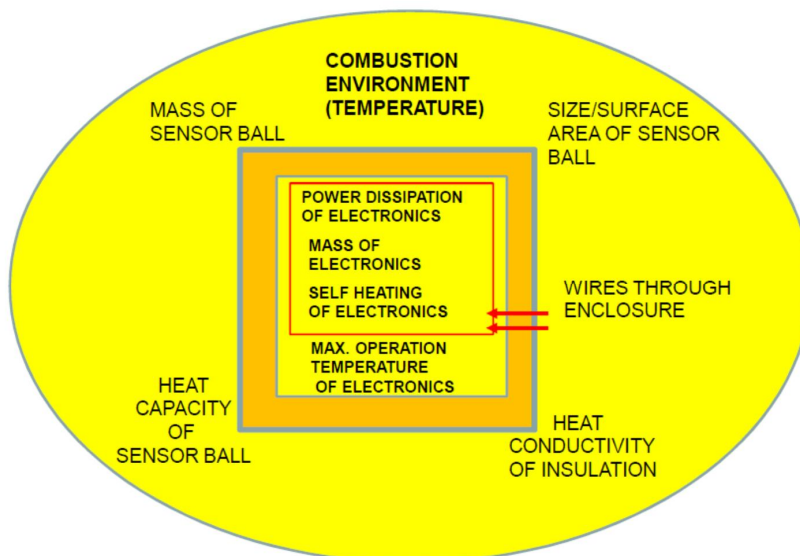

Figure 5.1: The operation time of a sensor ball in a combustion chamber depends on many contradictory factors. In addition, some factors directly affect the hovering of the sensor ball.

The operation time is dependent on the high temperatures in the combustion chamber, the properties of the sensor electronics, the maximum operation temperature of the electronics inside the sensor ball, and the thermal insulation of the enclosure around the sensor electronics. The temperature outside the sensor ball causes heat flow into the sensor ball in two ways: through the insulation walls and via wires led through insulations. Very rigorous requirements have been set for the insulation and physical dimensions of the ball. In addition, the hovering and operation time seem to be closely related to each other: the greater the mass of ball is, the easier it is to extend the operation time, but the more difficult is to make the ball hover, see chapter 6 and [Korhonen, 2017-2]. The mass can be higher if the size (cross-section) of the sensor ball can be increased. Increasing the size or surface area in turn increases thermal flow through the surface. The mass of the ball can be reduced if the heat capacity of the ball and its core can be increased or the heat conductivity of the thermal insulation can be reduced.

The following section deals with the theoretic background of heat capacity and heat conductivity. Subsequently, the importance of wires through a thermal insulator is studied. Finally, a practical solution for thermal protection and ideas for extending the operation time are presented.

5.2.1   Heat capacity, heat conductivity and heating

Heat capacity is the physical quantity of an object describing the relation between thermal energy led to the object and the temperature change of the object. The unit of heat capacity is J/K. Heat capacity can be given commensurate to mass, meaning specific heat or specific heat capacity, and its unit is J/K kg. Heat capacity is a complex function of temperature and material properties.

Heat or thermal conduction in a material is a consequence of two phenomena: migration of free electrons in metals or lattice vibrational waves in non-conducting materials. The quanta of lattice vibrations are seen as phonons. Thermal conductance k is a vector property of the material, defining the rate at which thermal energy is conducted in material. The heat conduction rate is defined by equation

$$\ddot{q} = -k\nabla T = -k \left(\boldsymbol{i}\frac{\partial T}{\partial x} + \boldsymbol{j}\frac{\partial T}{\partial y} + \boldsymbol{k}\frac{\partial T}{\partial z} \right), \quad\quad\quad (5.1)$$

where q is the heat flux (vector), k is the heat conductivity, T is the absolute temperature, and **i, j** and **k** are unit vectors in the directions x, y and z, respectively.

The equation shows that the heat flux vector is in a direction perpendicular to isothermal surfaces. The minus sign before k signifies that thermal energy flows in the direction of decreasing temperature.

According to kinetic theory, thermal conductivity can be expressed as follows [Incopera, 2007]:

$$k = \frac{1}{3} \, C \, \bar{c} \, \lambda_x \,, \qquad\qquad\qquad\qquad\qquad\qquad (5.2)$$

where C subtends in metals electron specific heat and in non-conducting materials the specific heat of phonons, $\bar{c}$ signifies in metals the mean electron velocity and in non-metals the average speed of sound in material, and λ_x signifies in metals the mean free path of electrons and in non-metals the mean free path of phonons. From the equation 5.2 it follows that thermal conductivity k is directly proportional to the mean free path and mean velocities of electrons or phonons. The electron or phonon specific heats are directly proportional to the absolute temperature. In contrast, the mean free path of electrons and phonons decreases with an increasing temperature.

In solid materials, k can be the sum of conductivity of electrons k_e and the conductivity of phonons k_{ph}:

$$k = k_e + k_{ph} \,. \qquad\qquad\qquad\qquad\qquad\qquad (5.3)$$

Thermal conductivity k depends on many material properties and phenomena, such as conduction and radiation in materials. All those phenomena as conductivity en bloc are temperature dependent. There are many models to describe it [Incopera, 2007; Zhao, 2012; Carson, 2005; Pietrak, 2015]. This thesis employs a general formula [Zhao, 2012]:

$$k = A_0 + A_1 T + A_2 T^2 + A_3 T^3. \qquad\qquad\qquad\qquad (5.4)$$

The coefficients A_0, A_1, A_2 and A_3 for the equation are specified according to empirical tests. Thermal coefficient k for insulation materials tends to increase with the temperature. Values for coefficients for the materials used in test sensor balls, see 5.2.4, are given in the next table:

Table 5.1: Coefficients to equation 5.4.

	A_0	A_1	A_2	A_3
POROMAX 26 BRICK	0.2187	0.0002	10^{-7}	$4*10^{-11}$
JM23 BRICK	0.1517	-0.0003	$5*10^{-7}$	$-3*10^{-10}$
SUPER-1100E BOARD	0.04	0.053	0.015	0.0017
WDS BOARD	0.0143	$5*10^{5}$	10^{-7}	0.0143
SMG-128 WOOL (SUPERMAG)	0.2295	0.0007	10^{-6}	$4*10^{-6}$

5.2.2 Self-heating

Self-heating of electronics is a consequence of power dissipation. Power dissipation originates from the dynamic operation of circuits and ohmic losses in quiescent states of circuits. In dynamic circuits, power dissipation is directly related to operation frequency. Power dissipation is less than the power consumption of electronics especially in transmitting devices because a part of energy fed into the transmitter is used for electromagnetic waves radiating from the antenna. The heating of electronics due to their own power dissipation is illustrated in Figure 5.2.
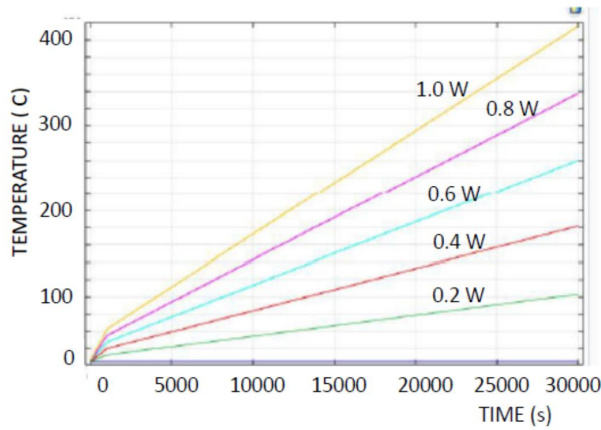
Figure 5.2: Heating of the inner chamber in 30000 seconds when the outside temperature is recursively set as the same as inside the chamber, at power levels 0.2, 0.4, 0.6, 0.8 and 1.0 W

Figure 5.2, which is the result of modelling by Comsol™, employs recursive heating, which means that the case temperature has been risen in all simulation rounds to the value of electronics in the earlier simulation round. In addition, heat losses out from enclosure are neglected. The heat capacity of the electronics is defaulted at 0.69 kJ/kg K and the mass of electronics is 25 g. The dissipation power was gradually set first to 0.2 W, then 1.0 W, and finally 0.2 W. According to the simulation, for example with the lowest power dissipation (0.2 W) the sensor warmed up to 100 ºC, near the point of destruction, in 30000 seconds or 500 minutes. At the dissipation power level of 1.0 W, the limiting temperature was reached in 3000 seconds or 50 minutes. In conclusion, the self-heating of the sensor must be taken into account if heating due to external temperatures takes tens of minutes. In addition, the mass and specific heat must also be taken into account when estimating self-heating.

5.2.3   Wires through envelope

Sensor wires, even thin ones, act as thermal conductors from high external temperature into envelope or towards sensor electronics. Thermal flow can be calculated with the equation

$$q = k\,A\,\frac{\Delta t}{\Delta x}\ , \qquad\qquad\qquad\qquad\qquad (5.5)$$

where k is the thermal conductivity of a wire, A is the cross-section of the wire, Δt is the temperature difference across the insulation and Δx is the thickness of the insulation (wire length inside it).

Table 5.2 contains results of calculations of heat flows via wires through insulation. In the calculations, the effect of insulation around the wire is neglected. Heat flow to the wire is defined by the effective surface of the wire to the external heat source and the absorption of the wire surface. According to measurements, the estimated specific heat energy of electronics is about 0.69 KJ/ Kg K. The rightmost column of Table 5.2 shows time estimates for over-heating (from 20 to 120 ^{o}C) of the sensor electronics due to thermal energy through wires, when the thermal source is seen infinite. The sensor electronics mass is defaulted at 25 g.

Table 5.2: Thermal power through insulator by a wire.

Metal type	Thermal Conductivity (W/K m)	Diameter (mm)	Heat flow (W) with infinite external thermal source	Heating time (s) from 20 to 120 ^{o}C
Copper (Cu)	393	0.5	3.27	405
Copper (Cu)	393	1.0	13.1	101
Steel (Fe)	58	0.5	0.48	2780
Steel (Fe)	58	1.0	1.94	684

According to Table 5.2, heat flow with a copper wire 1.0 mm in diameter from an infinite thermal source is about 13.1 W. This kind of flow heats the sensor core so much, that it directly affects the operation time of the sensor.

With an infinite external thermal source, the sensor electronics inside the insulator may overheat in as little as 101 seconds due to heat flow in a wire through the insulator. In practice, if only the head surface of the wire is open to external heat transport, the surface for heat exchange is about $7.85*10^{-7}$ m^2 and heat flow to the wire is 0.039 W to 0.157 W with finite external thermal sources from 50 kW/m^2 to 200 kW/m^2, respectively. Alternatively, if there is wire 10 mm in length with a diameter of 1 mm, the effective surface is approximately 0.000031 m^2 and the heat power is roughly 1.6 - 6.3 W with same external thermal power sources. In conclusion, thermal flow via wires through the thermal insulation must be taken into account in estimating the heating of electronics inside.

5.2.4   Modelling operation time in flames

To obtain a better understanding of operation times, the operation times were modelled and practical tests were conducted. For simulations and practical tests ball diameter was set to 95 mm and wall thickness to 20 mm. The modelling was performed with the Comsol™ Multiphysics Simulation tool, version 5. For both modelling and practical tests, five envelope materials was selected: Poromax 26 bricks, JM23 bricks, Super-1100E insulation board made by Skamol Ltd, WDS Porexherm insulation board and SMG-128 or SUPERMAG™ wool. In addition, a ball from pine wood was included in the tests due to interest. Table 5.3 lists the main parameters of five insulation materials relating to this study.

Table 5.3: Basic parameters of primary insulators used in the tests. Values missing from the list were not disclosed by the manufacturers.

Type	Density (kg/m^3)	Thermal conductivity W/ K m	Spesific heat kJ/ kg K	Max. operation Temperature $^{\circ}$C
POROMAX 26 BRICK	780	0.25-0.35		1430
JM23 BRICK	480	0.12-0.19	1.05	1260
SUPER-1100E BOARD	245	0.08-0.14	0.84	1100
WDS BOARD	226	0.02-0.045	1.05	1050
SMG-128 WOOL (SUPERMAG)	128	0.12-0.28		1200

The brick-like materials are quite porous and brittle. SMG-128 is wool-like material and WDS Porextherm is flocculent and packed between glass fibre coatings. Manufacturers' datasheets provide more accurate information concerning the tested materials.

Table 5. and Figure 5.3 show the thermal conductivities of the materials as functions of temperature. As stated earlier in this thesis, thermal conductivity is temperature related. Thermal conductivities of insulation material can increase three-fold in combustion temperatures compared to room temperature. Only thermal conductivity of WDS material seems to be quite stabile over the temperature area.
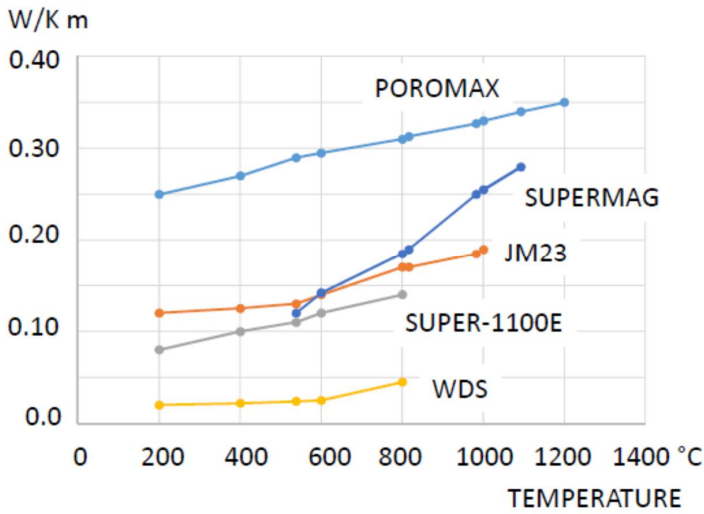
Figure 5.3: The thermal conductivity of insulators increases with temperature.

In the modelling, the external heat source is defaulted as infinite because the radiation and thermal flow (loading) in large combustors are high overall (50 – 200 kW/m^2), which means a heat flow of about 1272–5088 W to the ball surface. This means about 5 to 20 W energy to each area of one square centimetre on the ball surface. In comparison, raising the temperature of the sensor electronics (mass = 25 g, heat capacity Cp =0.677 kJ/kg K, ball diameter 95 mm) to 120 ^{o}C takes at shortest approximately 350 seconds in external temperature of 650 ^{o}C (see Figure 5.10, material SUPER-1100E). This temperature rise of electronics demands energy q= m* C$_p$ *Δt = 1.692 kJ. Most of this energy is transferred through the enclosure in 350 seconds or at power P = 1692 Ws/ 300 s = 4,834 W. Divided over the whole surface of the ball, the energy gives 0.0199 W/cm^2 , which is about 0.4 % of the power radiated and conducted to the ball surface.

The five above-mentioned materials and wood for comparison were modelled and simulated for a temperature increase inside the sensor ball. The following figures present a sample of the heat distribution in each material:
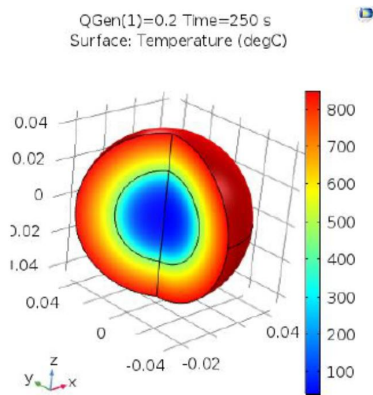
Figure 5.4: Heating in a ball made from SKAMOL SUPER-1100E. Situation 250 seconds from the start.
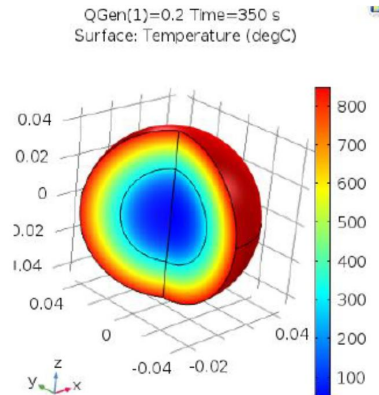

Figure 5.6: Heating in a ball made from POROMAX brick material. Situation 350 seconds from the start. Estimated heat capacity of enclosure material 1.2 kJ/ kg K.
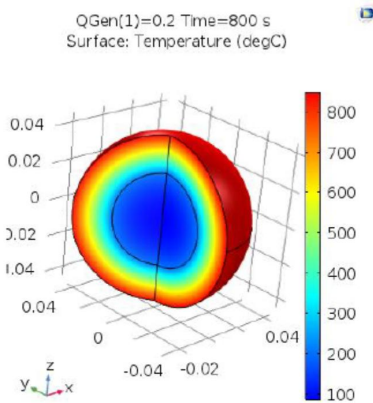

Figure 5.5: Heating in a ball made from WDS Porextherm. Situation 800 seconds from the start.
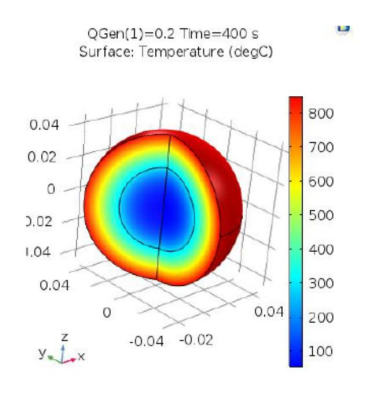
Figure 5.7: Heating in a ball made from Morgan JM23 brick material. Situation 400 seconds from the start.

QGen(1)=0.2 Time=170 s
Surface: Temperature (degC)


QGen(1)=0.2 Time=350 s
Surface: Temperature (degC)

+
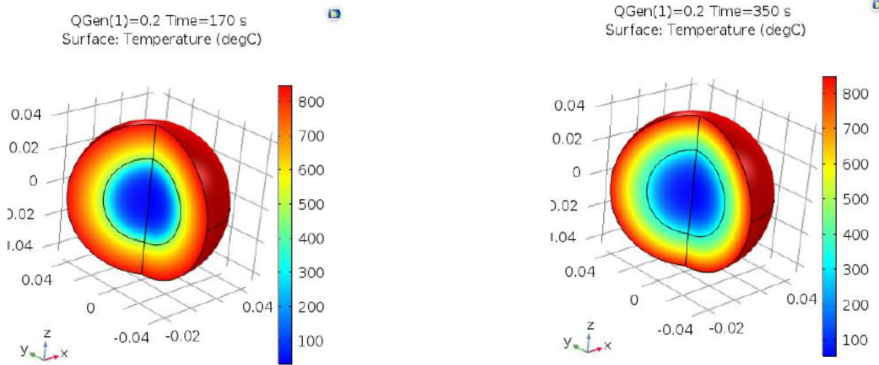
Figure 5.8: Heating in a ball made from SuperMag wool material. Situation 170 seconds from the start. Estimated heat capacity of the enclosure material 0.7 kJ/kg K.

Figure 5.9: Heating in a ball made from pine wood. Situation 350 seconds from the start. Estimated heat capacity of the wood material 1.5 kJ/kg K, heat conductivity 0.18 W/m K and density 380 kg/m3.

The inside temperatures in the balls are the same in all figures. For SuperMag wool and Poromax brick material, some parameters had to be estimated because they were not available; see figure texts. In all simulations the internal dissipation power was set to be 0.2 W and external temperature 850 °C.

Simulations showed clear differences between materials, as Figures 5.11 and 5.12 clearly indicate, representing summarized results of simulations at temperatures of 650 °C and 900 °C of balls having wall thickness of 20 mm and heat capacity of core 690kJ/Kg K.
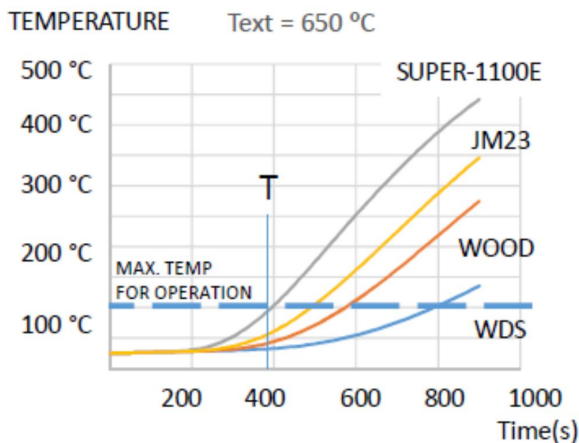

Figure 5.10: Heating of ball cores at an environment temperature of 650 °C according to simulations. Materials missing principal parameters are excluded from these simulations.
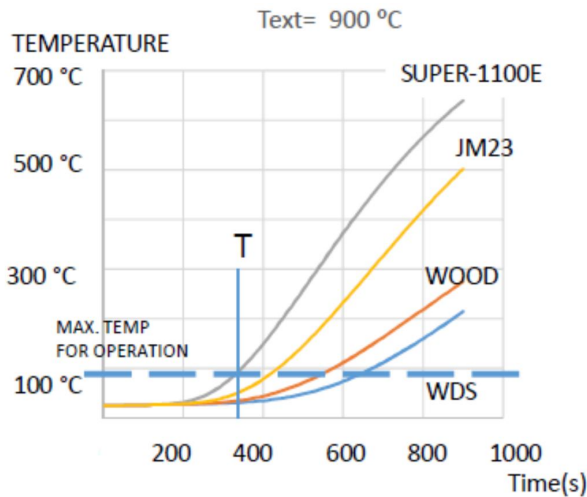
Figure 5.11: Heating of ball cores at an environment temperature of 900 $^{\circ}$C according to simulations. Materials missing principal parameters are excluded from these simulations.

The simulations suggest that WDS Porextherm would be the best, offering an operation time of approximately 900 seconds at a 650 $^{\circ}$C environment temperature and about 720 seconds at a 900 $^{\circ}$C environment temperature. The light material SuperMag wool seems to have the shortest lifetime: 300-400 seconds. The results clearly demonstrate the effect of the heat capacity, heat conduction factor and density in defining the protection.

5.2.5   Practical operation time tests

For the experimental tests a set of sensor balls with electronics were manufactured. The diameter of balls manufactured from bricks (JM23 and Poromax-26) and Super-1100E board was about 95 mm. Enclosures prepared from SMG-128 Supermag wool and WDS boards were tooled into rectangular, layered structures, having dimension of 95 * 95 * 95 mm^3. The wall thickness of the balls and layered structures was 20 $\pm$5 mm. Figure 5.12 displays the enclosures.

Figure 5.12: Sensor enclosures used in the test. Materials of the enclosures: In the bottom row, on the right SMG-128 wool and on the left WDS, in the upper row, from right to left, Super-1100E, Poromax26, JM23 and wood based enclosure halves

For the first tests in flames, sensor implementation was based on the ARDUINO™ Nano and HC-12 radio transceiver boards; see Figure 5.13. The combination was supplied from two lithium batteries type ER14250M, connected in series. The nominal voltage of the battery was 3.6 V. The size of the battery is half AA and its capacity 750 mAh. The battery was selected because it has quite a large loading current of 100 mA. This type of loading current is necessary for temporary high-load situations during data transmission from the sensor. Despite of the operating temperature range of this battery type is -40 to 85 ºC, it seems to tolerate operation at temperature of 120 ºC at least for minutes.
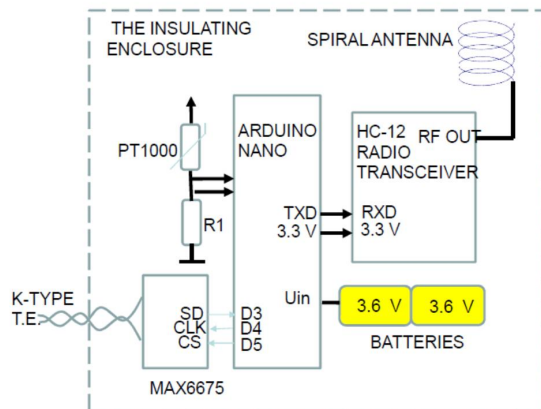

Figure 5.13: The test sensor was implemented by Arduino Nano, HC-12 and optionally MAX6675 K-type thermo element input modules. In addition, there were batteries and temperature sensor (PT1000).

The sensor electronics was assembled inside enclosure, in a pit drilled in sensor ball covers, see
Figure 5.14
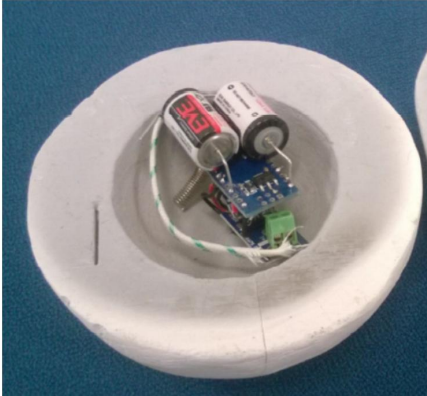
Figure 5.14: Electronics of the mobile sensor in an open enclosure

To measure the temperature inside the enclosure, the temperature sensor PT1000 was connected to the analog-digital converter input of the microprocessor. The sensor was a PT-1000 thermistor, type DM-507, manufactured by Labfacility Ltd. The operating temperature range of PT-1000 components is from -50 to 500 ºC. The nominal value at a temperature of 0 ºC is 1000 Ω. The temperature coefficient is 38.5 Ω / 100 ºC. The resistor R1 has a value of 1000 Ω.

The communication sensor electronics included a HC-12 transmitter module. The module operated at a 433 MHz frequency band. The output power of the module is selectable. In the test, a power level of 100 mW or 20 dBm was used. The module is connected to Arduino's microprocessor with a serial interface. The used bit rate of the interface was 9600 bit/s.

For the Arduino Nano module, a program was coded by Arduino C. The code was loaded into Arduino's memory by the USB interface of the board. The code is a loop base code. It reads the voltage from the voltage divider R1-PT1000 with an AD converter, packages voltage values into the message and transmits the message to the HC-12 module.

Some of sensors were equipped with external temperature measurement to determine the temperature around the sensor. The temperature sensor was a K-type thermoelement [Scervini, 2009]. It was connected to the system by a module containing a MAX6675 thermo-element adaptation circuit. The module implemented cold junction compensation automatically in the signal. It had a connector for thermos-element wires. The module communicated by a simple SPI protocol with the microprocessor.

In the first tests, receiver module was same kind of HC-12 module. It is connected by USB-to-serial converter module to PC or laptop. VisualStudio C++ based software was used to decode and scale measured values from messages. After decoding data was stored to text file. From the text file the values were moved to Excel file manually for post-processing. In first tests no positioning was needed nor used.

In test phase, the sensor balls were inserted into the small test combustor shown in Figure 5.15. The combustor was made from a concrete dwell ring with a diameter of about one metre. Pellets and wood were used as fuel. Air was supplied pressurized from under the grate.

Figure 5.15: Test combustor

The temperature in the bottom of the combustion chamber varied from roughly 650 to 908 ºC, see Figure 5.16. Sensor balls to be tested were kept about 100 mm over the combustion bottom, mainly inside flames. The actual temperatures around the sensor balls were not measured, but only estimated to be about 600 to 700 ºC.
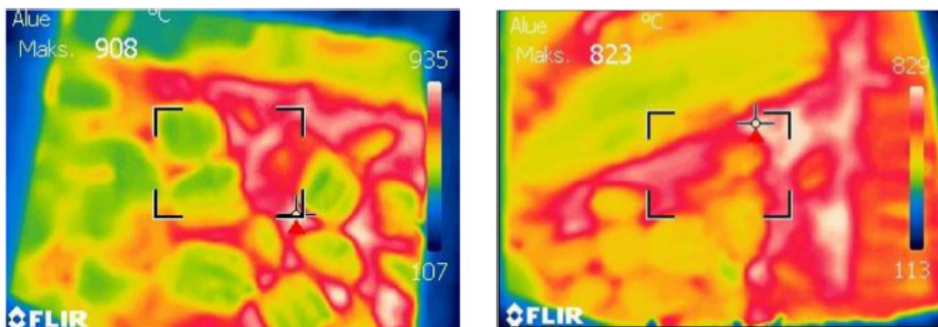

Figure 5.16: Temperature in the bottom of the test chamber varied from 650 to 908 ºC. The IR photos were taken with IR camera type FLIR T200. The emission factor in camera settings was set to 0.7 during measurements.

Figure 5.17 illustrates the results from the empirical tests. It's underlined, the results are tentative and there are many inaccuracies. The ball cores were heated with sensor

electronics introduced in section 5.2.5. Each curve represents a specific material and ends where the operation of electronics stopped inside the enclosure made from that material.

TEMPERATURE INSIDE SENSOR
(C)
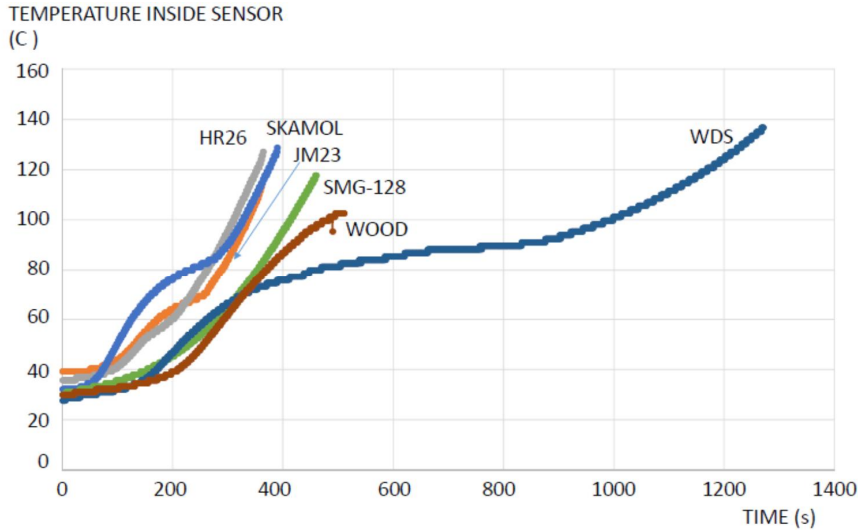
Figure 5.17: Heating of ball cores according to practical tests. Temperature around sensor balls was estimated to be about 600 to 700 °C.

The results of the empirical tests correlate well with the simulations introduced earlier. In the enclosure made of WDS Porextherm, the sensor operation stopped at about 137 °C after approximately 1300 seconds or 21 minutes of placing the sensor into the flames in the test combustor. The difference between simulations and empirical tests was largest in SMG-128 (SuperMag) wool. The operation time was longer in the experimental tests than in the simulations. The same occurred with the WDS material. In both cases, the declaration could be in enclosure materials. The walls of enclosures were in certain places thicker than 2.5 cm, and the enclosures from these materials were rectangular, while other enclosures were spherical; see Figure 5.12.

5.2.6   Extending operation time of sensor ball

The operation time can be extended by optimizing the power consumption of electronics and thermal properties of the comprehensive solution. Thermal properties such as the heat conductivity of insulation can be decreased and the heat capacity of insulation increased with better materials available or coming on the market. The heat capacity of the core can be increased by adding material with a high heat capacity value to the core. In the future, extending the temperature area of electronics (see section 5.1) can dramatically improve the operation time. All solutions must be proportioned to the mass and cross-section of the sensor ball to guarantee the best possible hovering of the sensor ball.

The figures 5.18- 5.24 represent simulations in which the enclosure thickness and core heat capacity vary. The basic parameters and material (Super-1100E) are the same is as in Figure 5.4.
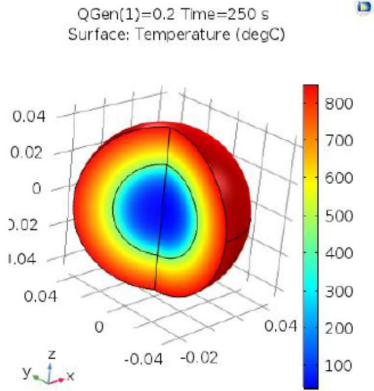
Figure 5.18: Basic situation. Mass of sensor ball approximately 100 g. Operation time 250 s.
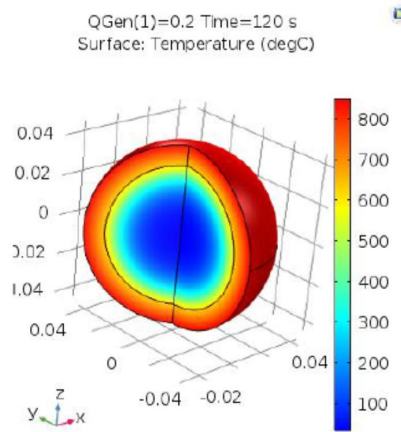
Figure 5.19: Wall thickness decreased to 10 mm. Mass of solution approximately 74 g. Operation time 120 s.
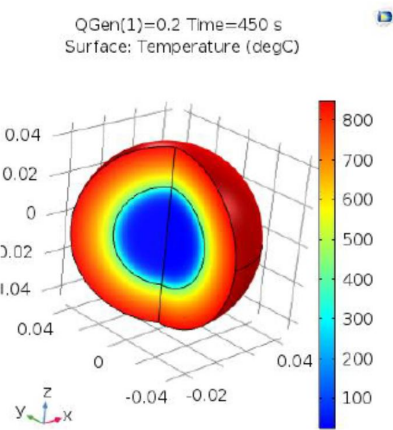
Figure 5.20: 50 g material with a heat capacity of approx. 4 kJ/kg K added to core. Lifetime increases to 450 s. Mass of solution 0.157 kg.
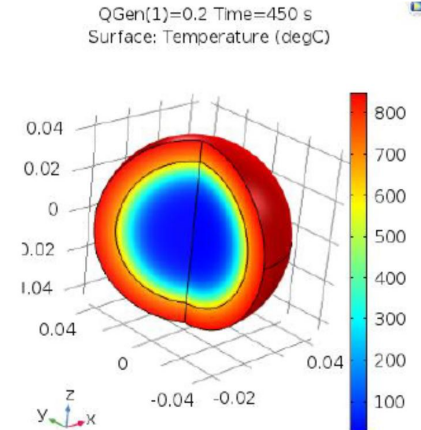

Figure 5.21: Wall thickness decreased to 10 mm. Operation time perhaps slightly shorter than in previous figure. 50 g high thermal capacity material at core. Mass of ball 0.124 kg.

QGen(1)=0.2 Time=450 s
Surface: Temperature (degC)
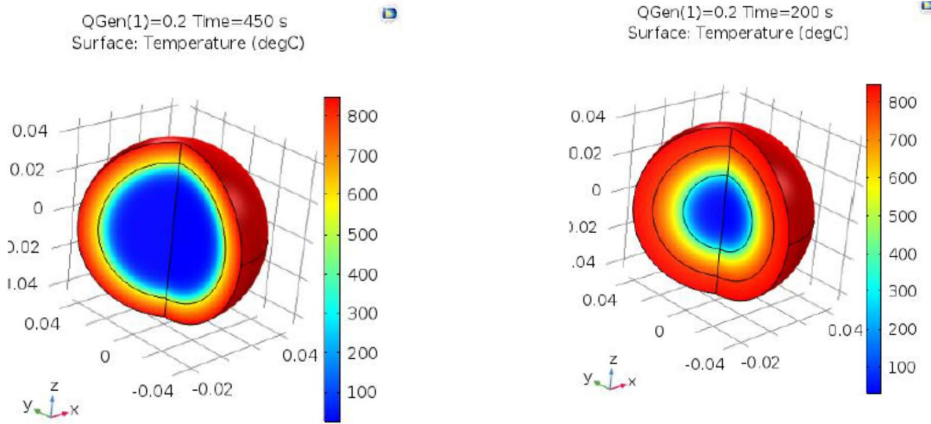
Figure 5.22: Wall thickness 10 mm. Operation time longer (450 s) than in previous figures. 75 g high thermal capacity material at core, total core mass 100g. Mass of ball 0.149 kg.

QGen(1)=0.2 Time=200 s
Surface: Temperature (degC)

Figure 5.23: Wall thickness 10 mm, core mass 25 g, total mass approx. 75 g, air gap added between core and enclosure. It extends operation time to 200 s.

QGen(1)=0.2 Time=250 s
Surface: Temperature (degC)
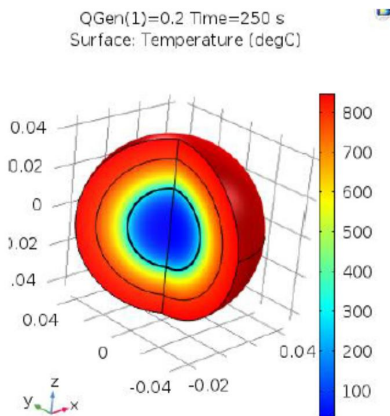
Figure 5.24: As in previous figure, but with aluminium foil of 0.5 mm thickness added around the core. Operation time extended to 250 s.

According to the simulations, varying the enclosure thickness both the operation time and the mass of the enclosure is highly controlled. An air gap alone and an air cap with aluminium around the core decreasing the radiative heat transfer will increase the operation time. In summary, the ball can be optimized with material and structural arrangements.

As summary, the operation time of the sensor seems to be in the order of minutes. Sensor structure, properties of insulation materials, heat capacity of core (electronics), wiring through insulation and external temperature all together define the operation time. In addition, power dissipation of the sensor electronics must be limited to about some hundreds of milliwatts in order to avoid self-heating and self-annihilation of the sensor.

6   Hovering of the sensor ball

Hovering of the sensor ball is key-issue to the sensor which is intended to propagate in all parts of combustion area. There are some ideas to use the ball as a bottom or non-hovering sensor. In this kind of applications, as for example measuring temperature of the heap in KRB boilers, hovering of the ball is to no purpose. In this chapter hovering issues are shortly discussed by theory and modelling base. Wider investigation of the issues are given in [Korhonen, 2017-2].

6.1   Theory of hovering

An object hovering freely in a medium, air, water, suspension, etc., is affected by three forces: drag F_D, buoyage F_B and gravitation force F_G. In a combustion environment, flows mainly move vertically; see Figure 6.1.
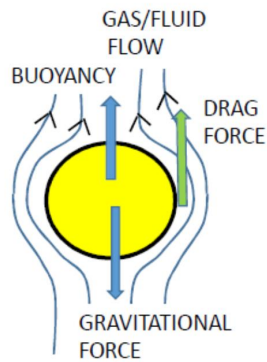

Figure 6.1: Forces acting on a hovering object.
.

To hover vertically, the forces affecting the object must be in balance, or

$$F_G = F_d + F_B. \tag{6.1}$$

The gravitation force is defined as a product of mass m of the object and Earth's gravity g, or

$$F_G = mg. \tag{6.2}$$

The object in a medium experiences lift or buoyancy according to the Archimedes law, which says that the object which is partially or completely embedded in a fluid will be lifted up by a force F_B which equals the weight of the fluid the object is displacing. So, the buoyancy can be defined as

$$F_B = V \rho g , \tag{6.3}$$

in which V is the volume of the object embedded in the fluid and ρ is the density of the fluid.

If the fluid around the object is in movement, the viscosity of the fluid, which is analogous to friction between solid objects, imposes a drag force F_D on the object. This drag force is calculated in two different ways relating to turbulence and the velocity of the fluid. For this reason, fluids are classified according to a dimensionless Reynolds number, which is defined as a ratio between the inertia forces and viscous force of the fluid with the following equation:

$$Re = \frac{\rho u L}{\mu} , \tag{6.4}$$

in which ρ is the density of the fluid, u is the characteristic velocity between the fluid and object, L is the characteristic linear length, and μ is the viscosity of the fluid.

When the flow of the fluid is non-turbulent, its Reynolds number is small – under 2000. If the Reynolds number exceeds 4000, the flow is turbulent. Between these limits is an intermediate area in which flow cannot be classified as non-turbulent or turbulent. For a spherical object, the drag can be calculated in a non-turbulent fluid using the Stokes equation

$$F_D = 6 \pi r \mu v, \tag{6.5}$$

in which r is the radius of the (spherical) object, μ is the viscosity of the fluid, and u is the velocity.

In turbulent flow conditions, drag is calculated related to the density of the fluid, viscosity and drag coefficient C_D:

$$F_D = C_D \frac{A \rho u^2}{2} . \tag{6.6}$$

In the equation, A is the nominal surface area of the object seen from the direction of the flow or the projected area. For a spherical object, it can be calculated with the following equation:

$$A = \frac{\pi \, d^2}{4},$$

(6.7)

in which d is the diameter of the sphere.

The drag coefficient is a dimensionless number. The coarseness of the object and compression of the medium at high velocities affect the drag force [Sadraey, 2009]. It has been defined through empirical tests for different objects. Table 6.1 provides examples of drag coefficient values [Engineering Toolbox].

Table 6.1: Examples of drag coefficients [Engineering Toolbox].

Type of object	C_D	Frontal area
Airplane wing, normal position	0.15	
Modern car e.g. Toyota Prius	0.26	
Truck	0.8- 1.0	
Train	1.8	
Rectangular box	2.1	
Sphere	0.45	$(\pi * d^2)/4$
Dolphin	0.0036	Wetted area

The drag coefficient of sand particles in CFB boilers is given in the following equation [Basu, 1992]:

$$C_D = \frac{a_1}{Re^{b_1}},$$

(6.8)

in which constants a_1 and b_1 can be approximated according to Table 6.2.

Table 6.2: Parameters for equation above [Basu, 1992]

Range of Re	Region	a_1	b_1
$0 <$ Re <0.4	Stokes law	24	1.0
$0.4 <$ Re < 500	Intermediate law	10	0.5
$500 <$ Re	Newton's law	0.43	0.0

In the region of Newton's law, substituting parameters to equation 6.8, a result of 0.43 is achieved. This is close to the value given for a spherical object in Table 1.

6.2 Practical considerations

To find out about the real hovering conditions, some simulations and calculations were carried out based on information collected on the issue. The study began by modelling and simulating velocity and pressure fields related to a ball hovering in a round channel with an air flow of 6 m/s. The diameter of the ball was 95 millimeters. The mass of the ball varies according to the enclosure wall density, which was set to 60 g for the modelling. Mass 60 g was chosen, because in the future work the goal is to tone up the sensor ball to 60 g. The simulation was performed with the Comsol™ 5.2 simulation tool using turbulent flow model. In simulations, the fluid temperature was set to 850 ºC, and the viscosity and fluid (air) densities were set to values present in that temperature or $4.1*10^{-5}$ Pas and 0.309 kg/m^3, respectively. Figure 6.2 shows the velocity field in the middle cross-section of the channel.
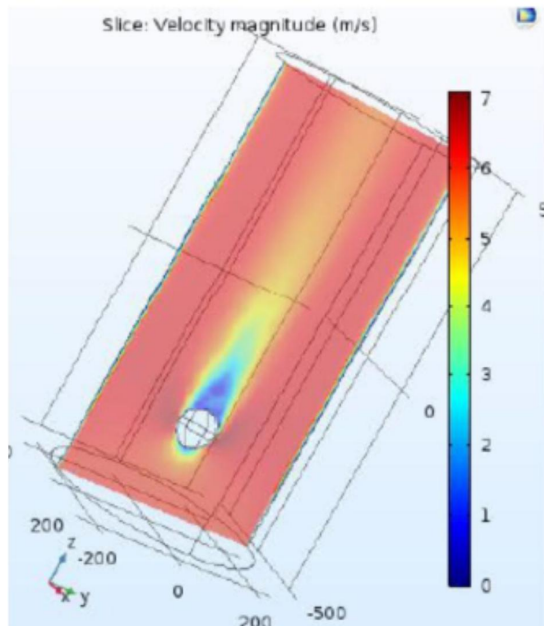
Figure 6.2: Velocity field around the sensor ball at an air flow speed of 6 m/s.

The simulation results indicated that in a narrow channel 500 millimetres in diameter, there was no wall effect at a velocity of 6 m/s or less. The tail of disturbance effects lasts over one meter above the ball.

An estimate was calculated for the hovering drag forces. In the hovering tests, only mass and size (diameter) of the sensor ball are known. The coarseness of the ball surface could not be taken into account in this study.

In the estimations, the ball was kept statically in position and rising flows from the bottom of a combustion chamber to the top were imagined. The ball properties were fixed, and only flow speeds and fluid or suspension densities varied in different areas of different boilers based on information introduced earlier in this thesis.

Figure 6.3 illustrates the results for a CFB boiler.
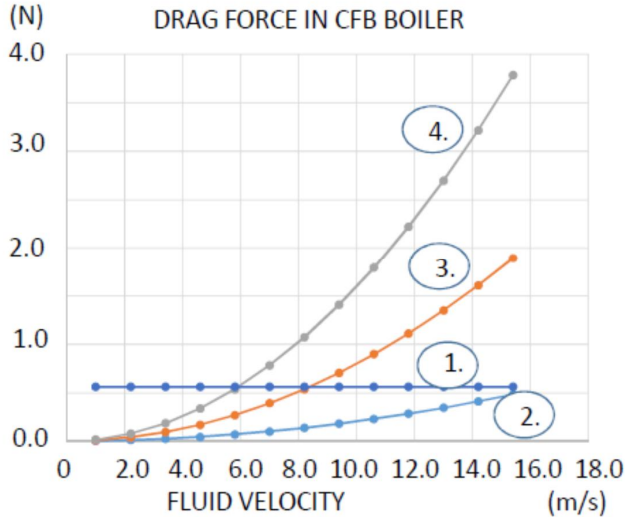
Figure 6.3: Gravity force and drag forces vs. fluid velocity in a CFB boiler. Curves: 1. Ball gravity force, 2. Fluid density 1,273 (kg/m3) = air, 3. Fluid density 5 kg/m3, 4. Fluid density 10 kg/m3.

Drag forces for a CFB boiler were calculated with fluid densities of 1.273 (kg/m^3), 5 kg/m^3 and 10 kg/m^3, because they represent air and typical densities in upper parts of CFB boilers. The calculated buoyancy forces are only 0.00285 N, 0.0119 N and 0.0223 N, respectively, at a fluid velocity of 6 m/s. The smallest density appears obviously in the flue gas channel of the CFB boiler. Other density values exist inside the chamber except in the bed, where the densities are about a decade higher. According to the graphs, at fluid densities greater than 10 kg/m^3, a ball with a mass of 60 g can hover when the fluid velocity is about 6 m/s. Velocities like this exist at least in so-called fast bed reactors, but sometimes also in ordinary CFBs. With smaller fluid velocities present in CFB boilers, the mass of the ball must be lighter or fluid densities greater. After all, one must keep in mind the down-coming suspension fluids in walls of CFB boilers. Sensor ball of whichever weight will be fallen down with these thick flows.

In BFB as in CFB boilers, the ball can hover only on top of the bed and just over it, in the splash area. In the free-board area in the BFB boiler, both fluid densities and fluid velocities are too low for hovering.

In kraft recovery boilers, the ball does not hover. On top of the char bed, the ball will adhere to the char bed material. Therefore, this sensor ball could be the first measuring device capable of measuring parameters on the char bed surface.

7   Sensor implementation future views

In paragraph 5.2.5, the sensor solution for practical tests was introduced. This chapter presents some visions concerning the future solution and work of the sensor ball, focusing on the positioning and communication issues.

7.1   Next generation sensor solution

The goal is for the sensor ball to operate in large combustion chambers, measuring, positioning itself and sending collected information in real time wirelessly to a receiver module.

According to the first studies, it seems that a self-positioning sensor would work best in a combustion area. This is based on the fact that all other principal positioning mechanisms, such as time of flight (ToF), time of arrival (ToA), time difference of arrival (TDoA), angle of arrival (AoA), and radio signal strength (RSSI), require a stable environment in relation to the speed of the radio signal, refraction and diffraction, and path loss. As stated earlier, the combustion environment does not fulfill the requirements of a stable environment. In principle, it could be possible to compensate for errors due to the above-mentioned unstable conditions, but it demands complicated reference systems and very intensive calculations.

The frequency band for wireless communications will be selected according to attenuation and noise issues; see sections 4.1 and 4.2. A balance seems to be needed between noise and attenuation forces to find a wireless solution, which has a link budget tolerating strong attenuation and has a narrow operation bandwidth to minimize limitations due to noise. Due to strong attenuation, the receiving system may demand a multi-antenna and/or multi-receiver solution to receive sensor transmission from all parts of the large boilers.

Many features are expected of measurements or sensors connected to a sensor ball. This thesis only states that the SPI interface and AD converters are the natural interface techniques for new sensors in final sensor electronics solutions.

The figure below illustrates a next generation sensor electronics solution.
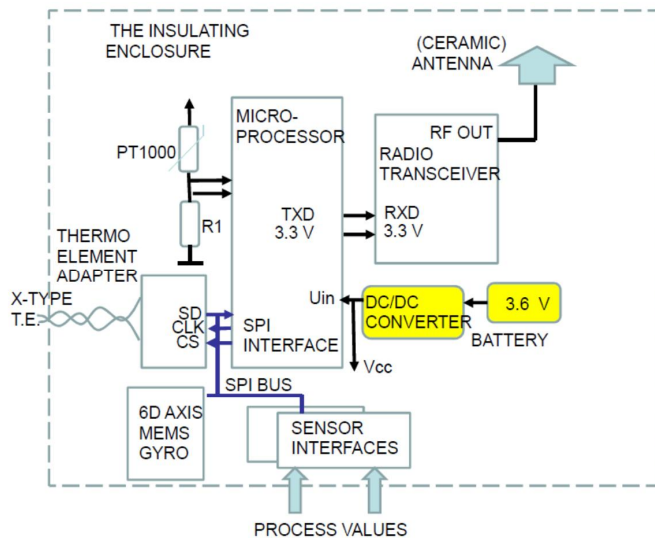
Figure 7.1: Next generation sensor electronics platform.

The main change compared to first phase sensor electronics is that the solution will be one printed board (PCB) solution. The microprocessor will be an 8 or 16 bit microprocessor having suitable interfaces. The next generation solution of sensor electronics must be lighter than the present one, with a mass of roughly 29 g. A switching power supply and one battery with a mass of about 10 g, is enough for suppling the system. Sensor electronics will include a 6D axis gyro/accelerator sensor for measuring rotations and positive and negative accelerations. This information is sent to the base station, in which software integrates trajectory and measurement information received from the ball and maps the data to a 3D transparent figure of the boiler.

7.2 Some views to measurements by the sensor ball

The usability of new sensors included in the sensor ball will mainly demand the limitation of the size and mass of the sensor and the response time of the measurement solution. The mass will be defined as the ratio between the sensor ball size and the sum of the intrinsic mass and increase of the mass due to new sensors. The response time is relative to the movements of the ball. It can be estimated that there will less static but more sudden dislocations. The response times of the sensors must be of the order which does not make identifiable or remarkable spatial errors in combining sensors and position results.

The energy usage of the new sensor is less remarkable due to superior battery technologies.

Temperature measurements are the main measurements. They must be based on thermoelement technology. Thermoelements demand their own connection solution to compensate for or avoid cold-junction errors. In addition, errors due to thermal radiation to and from elements must be compensated. Thermoelements are manufactured to temperatures of up to 1600 - 1800 ºC. Sensors having the highest temperature area suffer from increasing inaccuracy due to their relatively smaller thermoelectric voltage-temperature ratio.

Pressure measurements will be principally solved by small capacitive sensors. The inlet of gases to the pressure sensor must be protected against heat and dust. The inlet can primarily define the delay of the measurement because the response time of new sensors is of the order of milliseconds [SMI, 2017]

In the future, gas analysers based on micro-opto-electrical-mechanical systems (MOEMS) will obviously offer solutions for real-time gas analysis with a sensor ball [Hodkinson, 2013; VTT, 2017].

For sensors measuring process data, interface circuits are selected according to the requirements of the sensor itself. The most significant problems in new sensor technologies will be the mass of sensors, sampling of gases and energy demand. In the first hand, miniature pressure and obviously an ionisation meter are included in the sensor.

8 Discussion

The boiler environment is a multidisciplinary research object with challenges involving micro, nano and macro level phenomena. Combustion in itself is a complicated entity. To respond to all challenges arising from increasing boiler sizes, new fuels (such as waste and biofuels) and requirements for cleaner combustion, combustion phenomena and measurement need to be understood better. Radio and microwave based measurements and a mobile sensor are examples of promising new techniques in measuring combustion phenomena.

The first issue limiting all measurements – especially radio and microwave measurements – is that boilers are closed vessels with few small or no holes on the walls and roof. The lack or small size of holes hinder the use of sufficiently large antenna structures for wide band measurements, especially at radio wavelengths under one gigahertz. Dipoles as narrow bans antennas could be inserted into the boilers through instrumentation holes. They work well for narrow band sensor communication, but not for any wideband measurements.

According to the investigations, the communication solution must achieve a balance between three issues: noise in combustion, attenuation due to ionisation, and an adequate data rate (bit/s). The noise represents a challenge especially for wide bandwidth solutions. In flame temperatures above 800 - 900 ºC, the noise from black body radiation reaches levels which exceed the sensitivity of the receivers having a wide bandwidth preamplifier stage. Commercially available techniques of this type include e.g. Bluetooth and WLAN technologies.

The attenuation, which in a KRB is roughly 10 dB/m, can hinder the communication in large boilers completely. The plasma frequency, as stated in section 4.1, depends on the ionization degree in combustion. Consequently, the receiver and transmitter used must together offer and tolerate a path loss of approximately 120-140 dB or more in large combustion chambers. The attenuation may be slightly easier for other boiler types, but it needs to be verified through research. The bandwidth requirements correlate with the bit rate requirements of communication links. The bit rate is a function of the position data accuracy, sensor data amount, and update interval. The update interval depends mostly on requirements for the precision of positioning data. The amount of positioning data is dependent on the rotations and propagation velocity of the sensor ball. If the minimum update and communication interval is 50 milliseconds, the bit rate requirement with a minimum set of process values and position information is about 4000 bits/s.

Also the operation time is a function of contradictory issues. It mainly relates to the mass of the ball. According to the investigations, an operation time of minutes can be achieved,

but at the expense of hovering and propagation, excluding centre parts of CFB boilers, in which quite a massive ball can move freely. The simulations (see section 5.2.6) demonstrate that the operation time can be slightly adjusted in relation to the mass of the ball with some structural, core heat capacity and insulation related actions.

The final challenge is the hovering of the sensor ball. As mentioned in the previous chapter, hovering is an issue strongly related to operation time. In principle, hovering is a function of four main issues: the mass and cross-section of the ball, and suspension densities and flows inside combustion chambers. In CFB boilers, it is quite easy to make the ball hover due to moderate flow speeds and remarkable fluid densities. In other boilers, fluid densities are so low that special arrangements are needed to make the ball hover. One such arrangement is to sacrifice operation time. The mass of the sensor electronics is easily decreased to 10-15 g. However, it mostly depends on process sensor structures. With a light enclosure weighing around 10 g, the sensor ball can hover in many boilers. In this case, according to modelling, the operation time will be in the order of 20 seconds.

Further research is needed in this topic area. The positioning of sensors requires examination. At the system level, an antenna solution suitable for a combustion environment must be developed. This can occur after the frequency for the communication link is defined. Other topics that merit further study include, for example, a mathematical and software solution for representing measured, position related process values in a 3D transparent figure of a boiler. Following in the path of previous studies, researchers and designers continuing sensor ball development can focus on new measurement solutions to make the sensor ball a finalized, versatile new measurement device for combustion monitoring and measurement.

9   Conclusions

This thesis examined the behaviour of radio and microwaves and the phenomena behind them. In addition, the thesis studied the principal issues concerning the development of a mobile sensor ball propagating and measuring inside a combustion chamber, including operation time, hovering, measurement and communication.

The behaviour of electromagnetic waves is defined by chamber properties (size and wall materials) and ionisation, which is related to combustion activity, ionisation, fuels burned, and supplements in fuels. This thesis investigated the noise level and attenuation. According to practical tests in a kraft recovery boiler at Stora Enso Varkaus, the noise level in a KRB at frequencies of 0.1-19 GHz varied from -115 dBm to 100 dBm. Measurements were conducted by a spectrum analyser with a resolution bandwidth of 1 kHz and video bandwidth of 1 kHz. This principal noise level will remarkably affect the measurement and communication system using wide bandwidth receivers. This result means that e.g. such common techniques as WLAN and Bluetooth cannot be used in combustion environments. The attenuation of microwaves was measured in the same KRB. The attenuation during normal operation (black liquor burning) was measured to be about 10 dBm/m at frequencies from 2 to 18 GHz. Attenuation under the plasma frequency could be higher, but in the measurements, the actual plasma frequency could not be detected. The measured attenuation, approximately 10 dBm/m, means that in large boilers (largest dimensions over 40 m) the mobile sensor cannot communicate with a single antenna, but the communication system demands many antennas for receiving signals from mobile sensors.

The operation or lifetime of a sensor ball in a combustion area was preliminarily investigated by simulations, modelling and practical tests in a small-scale combustor. The operation time is related to the sensor ball size, wall material and its thickness, thermal conductivity, and the heat capacity of the wall material and sensor core. The operation time is ultimately closely connected to the hovering. In the tests, the limit for proper operation conditions for electronics was set to 120 °C. Six enclosure materials were investigated. According to the preliminary simulations and tests, the sensor ball can tolerate flames from about 4 to 10 minutes depending on the enclosure materials. The results must be seen as tentative due to many inaccuracies in the test arrangements.

Hovering issues of the sensor ball were tentatively calculated and simulated. Balls with a mass of about 29 g and diameter of 95 mm can hover in a CFB boiler riser area. In other boilers, hovering is possible only on the bubbling bed in a BFB boiler or on the char bed in a KRB.

Sensor electronics with temperature sensors for internal and external temperature measurement were implemented for the primary tests, using standard microprocessor and communications components. In the theoretical study, it was stated that active electronics

(such as microprocessors) for high temperatures are not yet available. In the second generation of sensor electronics, sensors must position themselves on six axes. In addition, versatile interfaces for gas and other sensors must be created and implemented.

After all, it seems that a mobile sensor ball capable of propagating and measuring inside industrial boilers is possible to implement. This work, although very preliminary, has paved the way for sensors that fulfil the requirements for new measurement tools, opening completely new measurement possibilities inside combustion chambers.

References

(Abihdima, 2010). Abihdima, A.M, Saleh, I.M. (2010). Effect of sand and dust storms on microwave propagation signals in southern Libya. ISBN *978-1-4244-5795-3/10. IEEE*. pp. 695- 698.

(Abdulla, 1988). Abdulla, S., Al-Rizzo, H., Cyril, M. (1988). Particle-size distribution of Iraqi sand and dust storms and their influence on microwave communication system. *IEEE Transactions on Antennas and Propagations,* 36(1), pp. 114-126.

(Adams, 1988) Adams, T., Frederick, W. (1998). Kraft recovery boiler physical and chemical processes. *American Paper Institute, Inc. New York, USA*.

(Agilent, 2006) *Basics of measuring of dielectric properties of materials.* Application note. Agilent Technologies. Listed from http://academy.cba.mit.edu/classes/input_devices/meas.pdf at 26.9.2017. p. 32.

(Agueda, 2010) Águeda, M., Pastor, E., Pérez, Y., Planas, E. (2010). Experimental study of the emissivity of flames resulting from the combustion of forest fuel. *International Journal of Thermal Sciences,* 49(3), pp.543-554.

(Aikio, 2011) Aikio, A. (2011). *Introduction to the ionosphere*. Dept. Physics, University of Oulu, Finland. p. 26.

(Atchison, 2003) Atchison, W. (2003). Impact of measurement System Noise Figure and Gain on emissions Measurements above 1 GHz. *Marconi Communications. IEEE,* Texas, USA. pp. 353-356.

(Basu, 2006) Basu, P. (2006). *Combustion and Gasification in Fluidized Beds*. ISBN 0-8493-3396-2. Taylor &Francis. USA. p.473.

(Batidzirai, 2013) Batidzirai, B. (2013). *Design of sustainable biomass value chains*. Doctoral Thesis. ISBN 9789086720569 Utrecht University. Netherlands. p.382.

(Braasch, 1999) Braasch, M., van Dierendonck, J. (1999). GPS Receiver Architectures and Measurements. Proceedings of IEEE, ~~Vol.~~ 87, No 1. Pp. 48-64.

(Carson, 2005) Carson, J., Lovatt, S., Tanner, D., Cleland, A. (2005). Thermal Conductivity bounds for isotropic, porous materials. *International Journal of Heat and Mass Transfer,* 48(11), pp. 2150-2158.

(Binner, 2014) Binner A., Lester, E., Kingman, S., Mathews J. et al. (2014). A review of microwave coal processing. *Journal of microwave power and electromagnetic energy,* 48(1), pp. 35-60.

(Blankinship, 2004) Blankinship, S. (2004). Microwave measurement can optimize coal-fired boiler combustion. *Power Engineering*, 108(10), p. 7.

(Boan, 2009) Boan, J.A. (2009). *Radio propagation in fire environments*. Doctoral Thesis. University of Adelaide. Australia. p. 228

(Bouet, 2008) Bouet, M., dos Santos, A. L. (2008). RFID Tags: Positioning Principles and Localization Techniques. Conference paper. *Wireless Days 2008*. p. 5.

(Coworker, 2017) Picture template listed 26.9.2017 from: org/electromagnetic-spectrum-visible-light-7b49746215112952.html

(Cyranka, 2016) Cyranka, M., Jurczyk, M. (2016). Energy recover from municipal waste based on moving grate technology. *Agricultural engineering*, 20(1), pp. 23-33.

(Demirel, 2012) Demirel, Y. 2012. *Energy and energy types. Energy, Green Energy and Technology*. Springer-Verlag Ltd., London, UK. p. 70.

(Engineering Toolbox)   Engineering Toolbox. www.engineeringtoolbox.com.

(Eriksson, 2004) Eriksson, H., Harvey, S. (2004). Black liquor gasification- consequence for both industry and society. *Energy,* 29(4), pp. 581-612.

(Fachberger, 2006) Fachberger, R., Bruckner, G., Hauser, R., Reindl, L. (2006). Wireless SAW based high-temperature measurements systems. *International Frequency Control Symposium and Exposition. 2006.* IEEE. p. 10.

(Fitzpatrick, 2013) Fitzpatrick, R. (2013). Electromagnetic waves in unmagnetized plasmas. *Lecture material of University of Texas at Austi*n. Web-address: http://farside.ph.utexas.edu/teaching/315/Waves/node63.html.

(Flinkenzeller, 2004) Finkenzeller, K. (2004). *RFID Handbook, Fundamentals and applications in Contactless Smart Cards and Identification*. ISBN 0-470-84402-7. 2nd edition. John Wiley & Sons Ltd. p. 427.

(Franke, 2003) Franke, J., Kral, R. (2003). Supercritical boiler technology for future market conditions*. Siemens product leaf.* Printed 25.4.2017: http://www.energy.siemens.com/mx/pool/hq/power-generation/power-plants/steam-power-plant-solutions/benson%20boiler-/Supercritical_Boiler_Technology_for_Future_Market_Conditions.pdf

(Green, 1964) Green, A.H., jr. (1964). A flame attenuation analysis using state-of-the-art millimetre techniques. *IEEE Digital Library*. pp. 172-181

(Hernando, 1999) Hernando, J., Perez-Fontan, F. (1999). *Introduction to mobile communications engineering*. ISBN 0-89006-391-5. Artech House, Norwood. p. 537.

[Hultgren, 2014] Hultgren, M., Ikonen, E., Kovács, J. (2014). Oxidant control and air-oxy switching components for CFB furnace operation. *Computers and Chemical Engineering,* 61, pp. 203-219.

(Incopera, 2007) Incopera, F., Dewitt, D., Bergman, T., Lavibe, A. (2007). *Fundamentals of heat and mass transfer*. ISBN-13 978-0-471-794714. John Wiley Sons. Asia. p. 925.

(Hachenberg, 2014) Hachenberg, N. (2014). *Prediction of NOx emissions in pulverized coal combustion.* Electronics Theses and Dissertations. Paper S57. p. 270.

(Halliday, 1997) Halliday, D., Resnick, R., Walker, J. (1997). *Fundamentals of physics, extended*. ISBN 0-471-10559-7. John Wiley& Sons. USA. p. 1142.

(Halpern, 1958) Halpern, C., Ruegg, F.W. (1958). A Study of sampling of flame gases. *Journal of Research at the National Bureau of Standards,* 60(1), pp. 29 - 37.

(Hansen, 2001) Hansen, H., Pedersen, A., Ottosen, L., Villumsen, A. (2001). Speciation and mobility of cadmium in straw and wood combustion fly ash. *Chemosphere* 45(1), pp. 123-128.

(Hauschild, 1995) Hauschild, T., Knöckel, R. (1995). Microwave Measurement of Density Profiles in Fluidized Bed Reactors with Improved Spatial Resolution. *Microwave Symposium Digest.*1995. IEEE MTT-S. pp. 1467-1470.

(Hauser, 2005) Hauser, R., Fachberger, R., Bruckner, G., Reicher, R., Smetana, W. (2005). Ceramic Patch Antenna for High Temperature Applications. *28th Int. Spring Seminar on Electronics Technology*. 2005. IEEE. pp. 159-165.

(Hernando, 1999) Hernando, J., Perez-Fontan, F. (1999). *Introduction to mobile communications engineering*. ISBN 0- 89006-391-5. Artech House, UK. p. 535.

(Heron, 2004) Heron, M.L., Mphale, K. (2004). *Radio wave attenuation in bushwires, tropical cyclones and other severe atmospheric conditions*. Final Report on EMa Project 60/2001. Australia. p. 35.

(Hodkinson, 2013) Hodkinson, J., Tatam, R. P. (2012). Optical gas sensing: a review. *Measurements Science Technology,* 24.

(Hornsteir, 1998) Hornsteir, J., Born, E., Fischerauer, G., Riha, E. (1998). Surface Acounctic Wave Sensors for High-Temperature Applications. *IEEE International Frequency Control Symposium.* 1998. IEEE. pp. 615-620

(Huhtinen, 2004) Huhtinen, M., Kettunen, A., Nurminen, P., Pakkanen. (2004). *Höyrykattilatekniikka*. ISBN 951-37-3360-2. Edita Oy. Helsinki. p. 342.

(Hui, 2009) Hu, H.T. (2009). *Plane Wave Propagation in Lossy Media (Intensive reading)*. Lecture Material. National University of Singapore. Printed 13.4.2017 from https://www.ece.nus.edu.sg/stfpage/elehht/Teaching/EE2011%20Part%20B/Lecture%20Notes/Intensive%20Readings%20-%20Optional/Plane%20Wave%20Propagation%20in%20Lossy%20Media.pdf

(Hulkkonen, 2006) Hulkkonen, S. (2006). CHP generation from biomass fuels. part2, Biomass fuels and conversion technologies. *5Eures International Training*. Joensuu. p. 44.

(Hurskainen, 2013) Hurskainen, M., Kärki, J., Korpijärvi, K., Leinonen, A., Ompola, R. (2013). Pajun käyttö polttoaineena kerrosleijukattiloissa. *Research report. VTT-R-06093-13*. VTT, Finland. p. 43.

(IEA, 2016) *World Energy Outlook 2016*. Executive summary. International Energy Agency (IEA).

(IFRF, 2009) *Measurement Equipment, Suction pyrometer*. Doc. No. C76/y/1/17b. IFRF.

(Jones, 2000) Jones, J. (2000). A combustion scientist view of thermocouple. *The institution of Electrical Engineers.* London, UK. p. 11.

(Järvinen, 2002) Järvinen, M. (2002). *Numerical Modelling of the Drying, Devolatilization and Char Conversion Processes of Black Liquor Droplets.* Doctoral Thesis. ISBN- 951-666-617-5. Helsinki University of Technology. Helsinki. p. 121.

(Kalisz, 2004) Kalisz, S., Pronobis, M. (2004). Investigations on fouling rate in convective bundles of coal-fired boilers in relation to optimization of sootblower operation. *Fuel*, 84(7-8), pp. 927-937.

(Kabilevich, 2011) Kabilevich, B., Litvak, B. (2011). Noise versus coherency in mm-wave and microwave scattering from non-homogeneous materials. *Progress in Electromagnetics Research B,* 28, pp. 35-54.

(Khan, 2009) Khan, A., de Jong, W., Jansens, P., Spliethoff, H. (2009). Biomass combustion in fluidized bed boilers: Potential problems and remedies. *Fuel processing technology,* 90(1), pp. 21-50.

(Kohse-Höinghaus, 2002) Kohse-Höinghaus, K., Jeffries, J.B. (2002). *Applied combustion diagnostics*. ISBN 1-56032-9013-0. Taylor&Francis. Great Britain. p. 705.

(Korhonen, 2017-1) Korhonen, I., Ahola, J. (2017). Microwave spectra inside the Combustion Chamber of Kraft Recovery Boiler- Effects to Communication. *IET Science, Measurement & Technology*. Doi:10.1049/iet-smt.2016.0384. p. 6.

(Korhonen, 2017-2) Korhonen, I., Laine, V. (2017). Estimating Hovering of a Mobile Sensor in Combustion Boiler Environment. *Measurement,* 109. pp. 100-104.

(Korhonen, 2017-3) Korhonen, I., Ahola, J. (2017). Estimating the Specific Heat Capacity of Electronic Devices. *IEEE Instruments and Measurements Magazine*. Accepted to publication. p. 16.

(Korhonen, 2017-4) Korhonen, I., Ahola, J. (2017). Microwave attenuation in Kraft recovery boiler. *IET Microwaves, Antennas & Propagation.* DOI: 10.1049/iet-map.2017.0263. p. 8.

(Lackner, 2013) Lackner, M., Palotas, A., Winter, F.(2013). *Combustion. From Basics to applications*. ISBN 978-3-527-33376-9. Wiley-VCH, Austria. p. 269.

(Letsholathebe, 2014) Letsholathebe, D., Mphale, K., Chimidza, S. (2014). Nondestructive Measurement of Momentum Transfer Collision frequency for Low Temperature Combustion. *International Journal of antennas and propagation.* Article ID 384701, p. 7.

(Letsholathebe, 2015) Letsholathebe, D., Mphale, K. (2015). Absorption of microwaves in low intensity eucalyptus litter fire. *Journal of Electromagnetic Analysis and Applications,* 7, pp. 217-224.

(Lind, 1999) Lind, T., Valmari, T., Kauppinen, E., Sfiris, G., Nilsson, K., Maenhaut, W. (1999). Volatilization of heavy metals during circulating fluidized bed combustion of forest residue. *Environmental Science Technology,* 33. pp. 496-502.

(Lipták, 2017) Lipták, B., Venczel, K. (editors) (2017). *Instrumentation and Automation Engineers' Handbook*. Volume 1. Measurements and Safety. Fifth edition. ISBN 13-978-1-4987-2764-8. CRC Press, Taylor & Francis. pp. 552-553.

(Ljung, 1997) Ljung, A., Nordin, A. (1997). Theoretical feasibility for ecological biomass ash recirculation: Chemical equilibrium behavior of nutrient elements and heavy metals during combustion. *Environmental Science Technology*, 31. pp. 2499-2503.

(Lu, 2007) Lu, Y., Lee, T. (2007). Influence of the feed gas composition on the Fischer-Tropsch synthesis in commercial operations. *Journal of Natural Gas Chemistry,* 16, pp. 329-341.

(Lumen) Electromagnetic waves and their properties. Listed 6.10.2017 from course material at https://courses.lumenlearning.com/boundless-physics/chapter/electromagnetic-waves-and-their-properties/.

(Mikkanen, 2000) Mikkanen, P. (2000). *Fly ash particle formation in Kraft recovery boilers*. Thesis. VTT Publications 421. Finland. p. 70.

(Miikkulainen, 2000) Miikkulainen, P., Järvinen, M., Kankkunen, A. (2000). Black liquor spray properties in operating recovery boiler furnaces. *INFUB 5th European conference on Industrial Furnaces and Boilers*, 2000. Portugal. p. 70.

(Miikkulainen, 2006) Miikkulainen, P. (2006). *Spray formation of high dry solids black liquor in recovery boiler furnaces*. Doctoral thesis, Helsinki University of Technology. ISBN-13 978-951-22-8507-5. p. 169.

(Moulzof, 2010) Moulzof, S., Behanan, R., Lad, R., da Cunha, M.P. (2010). Langasite SAW Pressure sensor for harsh environment. *UltraSonic Symposium*. IEEE International. pp. 1224- 1227.

(Mrosk, 2001) Mrosk, J., Berger, L., Ettl, C., Fecht, H-J., Fischerauer, G., Dommann, A. (2001). Material Issues of SAW Sensors for High-Temperature Applications. *IEEE Transaction on Industrial Electronics,* 48(2), pp. 258-264.

(Mphale, 2006) Mphale, K., Heron, M., Ketlhwaafetse, R., Letsholathebe, D., Casey, R. (2010). Interferometric measurement of ionization in a grassfire. *Meterology and Atmoshperic Physics*, 103(3), pp. 191-203.

(MPhale, 2006-2) Mphale, K., Heron, M. (2006). Plant alkali content and radio wave communication efficiency in high intensity savanna wildfires. *Journal of atmospheric and Solar-terrestrial physics,* 69(4-5), pp. 471-484.

(Mphale, 2007) Mphale, K., Letsholathebe, D., Heron. M. (2007). Effective complex permittivity of a weakly ionized vegetation litter fire at microwave frequencies. *Journal of Physics D: Applied Physics,* 40(21), pp. 6651-6656.

(Mphale, 2007-2) Mphale, K., Jacob, M., Heron, M. (2007). Prediction and measurement of electron density and collision frequency in a weakly ionized pine fire. *Int. J Infrared Milliwaves,* 28(3), pp. 251-262.

(Mphale, 2007-3) Mphale, K., Jacob, M., Heron, M. (2007). Absorption and transmission power coefficients for millimeter waves in a weakly ionised vegetation fire. *Int. J Infrared Millimeter Waves,* 28(10), pp. 865-879.

(Mphale, 2008) Mphale, K., Luhanga, P., Heron, M. (2008). Microwave attenuation in forest fuel flames. *Combustion and Flame,* 154. pp. 728-739.

 (NREL, 1997) *Alkali deposits found in biomass boilers*. A Joint effort. NREL/TP-433-8142. National Renewable energy laboratory. USA. 1997. p. 122.

(Penque, 2007) Penque, A. (2007). *Examination of chlorides in municipal solid waste to energy residue: origins, fate and potential for treatment*. MSc thesis. Columbia university. USA. p. 37.

(Pietrak, 2015) Pietrak, K.,Wisniewski, T. (2015). *A review of models for effective thermal conductivity of composite materials. Journal of Power Technology,* 95(1), pp. 14-24.

(Radicella, 2004) Radicella, S., Ryszard, R. editors. (2004). *Antennas Basics*. Chapter 4. Radio Laboratory Handbook. http://wireless.ictp.it/handbook/C4.pdf. Trieste.

(Rahmat-Samii, 1995) Rahmat-Samii, Y., Williams, L.I., Yaccarino, R.G. (1995). The UCLA Bi-Polar Planar-Near-Field Antenna-Measurement and Diagnostics Range. *IEEE Antennas and Propagation magazine*, 37(6), pp. 30-45.

(Raiko, 2002) Raiko, R., & co. (2002). *Poltto ja palaminen*. 2nd edition. ISBN 951-666-604-3. IFRF Finland National Organisation. Gummerus Ltd. Finland. p. 70.

(Ransom, 2016) Ransom, S. (2016) *Essential radio astronomy*. Appendix D: Wave propagation in plasma. http://www.cv.nrao.edu/~sransom/web/A4.html.

(Rao, 2011) Rao, X., Hemawan, K., Wichman, I., Carper, C., Grotjohn, T., Asmussen, J., Lee, T. (2011). Combustion dynamics for energetigally enhanced flames using direct microwave energy coupling. *Proceeding of the Combustion Institute,* 33, pp. 3233-3240.

(Rogalski, 2014) Rogalski, A., Chrzanowski, K. (2014). Infrared devices and techniques (revision*). Metrology and Measurement Systems*, 21(4), pp. 565-618.

(Sadraey, 2009) Sadraey, M. (2009). *Drag force and drag coefficient.* Chapter 3. Air Craft Performance Analysis. WDM Verlag Dr. Müller. Printed 27.4.2017: http://faculty.dwc.edu/sadraey/Chapter%203.%20Drag%20Force%20and%20its%20Coefficient.pdf.

(Savarese, 2002) Savarese, C., Rabaey, J. (2002). *Robust positioning algorithms for distributed ad-hoc wireless sensor networks. USENIX 2002*. pp. 317-327.

(Saviharju, 2006) Saviharju, K. (2006). *Method and apparatus for wireless measuring in closed space.* Patent WO2006048502, 11.5. 2006. Printed from: https://patentscope.wipo.int/search/en/detail.jsf?docId=WO2006048502

(Scervini, 2009) Scervini, M. (2009). *Thermoelectric materials for thermocouples*. University of Cambridge. Printed 25.4.2017 from

https://www.msm.cam.ac.uk/utc/thermocouple/pages/ThermocouplesOperatingP rinciples.html. UK.

(Shu, 2015) Shu, L., Peng, B., Yang, Z., Deng, S., Liu, X. (2015). High-Temperature SAW Wireless Strain Sensor with Langasite. *Sensors,* 15, pp. 28531-28542.

(SMI, 2017) *SMI Pressure Sensors, Medium pressure sensor digital output.* Datasheet. Listed at 27.9.2017 from http://www.hdi-electronics.fr/wp-content/pdf/SM3041.pdf.

(Steenari, 1999) Steenari, B-M., Lindqvist, O., Andersson, B-A. (1999). Preliminary characterization of deposits formed on super heater surfaces in an FBC-boiler fired with municipal solid waste. *Proceedings of the 15th international conference on fluidized bed combustion.* Savannah, Georgia.

(Stephan, 2004) Stephan, K.D., Pearce, J.A., Wang, L., Ryza, E. (2004) Prospects for industrial remote temperature sensing using microwave radiometry. *IEEE MTT-S International Microwave Symposium Digest,* 2, pp. 651-654.

(Stockman, 2009) Stockman, E., Zaido, S., Miles, R., Carter, C., Ryan. N. (2009). Measurements of combustion properties in microwave enhanced flame. *Combustion and Flame,* 156, pp. 1453-1461.

(Söderhjelm, 1994) Söderhjelm, L. (1994). Black liquor properties. *30 Years recovery boiler co-operation in Finland. International Conference Baltic Sea.*

(Thiele, 2005) Thiele, J., da Cunha, M-P. (2005). High temperature LGS SAW gas sensor. *Sensors &Actuators B: Chemical,* 113(2), pp. 816-822.

(Teir, 2003) Teir, S. & co. (2003). *Steam Boiler Technology.* 2nd edition, HUT. ISBN 951-22-6759-4, Helsinki. p. 216.

(Tourunen, 2013) Tourunen, A. (2013). *Development of high-efficiency CFB technology to provide flexible air/oxy operation for a power plant with CCS.* Project final report. VTT Finland.

(Tulonen, 2012) Tulonen, T., Arvola, L., Strömmer, R. (2012). Cadmium release from afforested peatlands and accumulation in an aquatic ecosystem, after experimental wood ask treatment. *European Journal of Forest Research,* 131(5), pp. 1529-1536

(Turner, 1994) Turner, R., Fuierer, P., Newnham, R. et al (1994). Materials for High Temperature Acoustic and Vibration Sensors: A Review. *Applied Acoustics,* 41(4), pp. 299-324.

(Ukkonen, 2006) Ukkonen, L. (2006). *Development of Passive UHF RFID Tag Antennas for Challenging Objects and Environments*. Doctoral thesis, Tampere University of Technology. ISBN 952-15-1659-3. p. 122.

(Utt, 2011) Utt, J., Giglio, R. (2011). Technology comparison of CFB versus pulverized-fuel firing for utility power generation. OFSA 2011, *Industrial Fluidization* South Africa. Johannesburg, South-Africa. pp. 91-99.

(Wang, 2013) Wang, L., Skjevrak, G., Hustad, J., Skreiberg, Ö. (2013). *Investigations on biomass ash sintering characteristics and the effect of additives. Energy&Fuels* 2014, 28. pp. 208-218.

(Vakkilainen, 2007) Vakkilainen, E. (2007). *Kraft recovery boilers- Principles and practice*. Valopaino Oy, Helsinki. ISBN 952-91-8603-7. p. 246.

(Vassilev, 2013) Vassilev, S., Baxter, D., Vassileva, C. (2013). An overview of the behaviour of biomass during combustion: Part II. Ash fusion and formation mechanisms of biomass types. *Fuel,* 117, pp. 152-183.

(Watteyne, 2010) Watteyne, T., Lanzisera, S., Mehta, A., Pister, K. (2010). Mitigating multipath fading through channel hopping in wireless sensor networks. *IEEE ICC2010 proceedings.* p. 5.

(Webber, 2000) Webber, M., Wang, J., Sanders, S., Baer, D., Hanson, R. (2000). In situ combustion measurements of CO, CO_2, H_2O and temperature using diode laser absorption sensors. *Proceedings of Combustion Institution*, 28. pp. 407-413.

(Werkelin, 2005) Werkelin, J., Skrifvars, B-J., Hupa, M. (2005). Ash-forming elements in four Scandinavian wood species. Part I: summer harvest. *Biomass and Bioenergy,* 29. pp. 451-466.

(Williams, 2001) Williams, K., Greeley, R. (2001). Radar attenuation by sand: Laboratory measurements of radar transmission. *IEEE Transactions on Geoscience and Remote Sensing,* 39(11), pp. 2521-2526.

(Williams, 2006) Williams, R.A., Beck, M.S. (2006). *Process tomography: Principles, Theory and Applications*. Butterworth Heinemann. ISBN 07506-0744-0. pp. 582.

(Vishvakarma, 1981) Vishvakarma, R., Rai, C.S. (1981). Limitations of Rayleigh scattering in the prediction of millimeter wave attenuation in sand and dust storms. *Banaras Hindu University*. India. pp. 267-269.

(Woodhouse, 2006) Woodhouse, I. (2006). *Introduction to microwave remote sensing*. ISBN 0-415-27123-1. Informa. Taylor @ Francis Group. USA. p. 400.

(Wright, 2003) Wright, I.G., Stringer, J., Wheeldon, M. (2003). Materials Issues in Bubbling PFBC Systems. *Materials at High Temperatures,* 20(2), pp. 219-232.

(Vouk, 1983) Vouk, V., Piver, W. (1983). Metallic elements in fossil fuel combustion products: Amounts and form of emissions and evaluation of carcinogenicity and mutagenicity. *Environmental Health Perspectives,* 47, pp. 201-225.

(VTT, 2017) *Optical microspectrometer. MOEMS FPI technology for microspectrometers and spectral imagers*. Technical information on Web side. Listed 27.9.2017 from http://www.vttresearch.com/services/smart-industry/process-and-analytical-measurement/optical-sensors.

(Yeh, 2007) Yeh, S., Rubin, E. (2007). A centurial history of technological change and learning curves for pulverized coal-fired utility boilers. *Energy,* 32, pp. 1996-2005.

(Zbogar, 2004) Zbogar, A., Frandsen, F., Jensen, P., Glarborg, P. (2004). *Heat transfer in ash deposits: A modelling tool-box*. CHEC Reasearch Group of chemical engineering. Technical University of Denmark. 2005. pp. 371-421.

(Zeng, 2011) Zeng, P., Chin, T-L., Greve, D., Oppenheim, I., Malone, V., Cao, L. (2011). High-Temperature Langasite SAW Oxygen sensor. *IEEE Transactions on Ultrasonic, Ferroelectronics, and Frequency Control*, 58, pp. 1538-1540.

(Zhao, 2012) Zhao, J-J., Duan,Y-Y., Wang, X-D., Wang, B-X. (2012) An analytical model for combined radiative and conductive heat transfer in fiber-loaded silica aerogels. *Journal of Non-Crystalline Solids,* 358. pp. 1303-1312.

(Zuo, 2016) Zuo, H., Long S., Wang, C., Zhang, P. (2016) A Review of Microwave Treatment on Coal. In: Hwang JY. et al. (eds) *7th International Symposium on High-Temperature Metallurgical Processing*. ISBN 978-3-319-48617-8. Springer, Cham. pp. 618-622.

ACTA UNIVERSITATIS LAPPEENRANTAENSIS

740. KÄHKÖNEN, TOMMI. Understanding and managing enterprise systems integration. 2017. Diss.

741. YLI-HUUMO, JESSE. The role of technical dept in software development. 2017. Diss.

742. LAYUS, PAVEL. Usability of the submerged arc welding (SAW) process for thick high strength steel plates for Arctic shipbuilding applications. 2017. Diss.

743. KHAN, RAKHSHANDA. The contribution of socially driven businesses and innovations to social sustainability. 2017. Diss.

744. BIBOV, ALEKSANDER. Low-memory filtering for large-scale data assimilation. 2017. Diss.

745. ROTICH, NICOLUS KIBET. Development and application of coupled discrete and continuum models in solid particles classification. 2017. Diss.

746. GAST, JOHANNA. The coopetition-innovation nexus: Investigating the role of coopetition for innovation in SMEs. 2017. Diss.

747. KAPOOR, RAHUL. Competition and disputes in the patent life cycle. 2017. Diss.

748. ALI-MARTTILA, MAAREN. Towards successful maintenance service networks – capturing different value creation strategies. 2017. Diss.

749. KASHANI, HAMED TASALLOTI. On dissimilar welding: a new approach for enhanced decision-making. 2017. Diss.

750. MVOLA BELINGA, ERIC MARTIAL. Effects of adaptive GMAW processes: performance and dissimilar weld quality. 2017. Diss.

751. KARTTUNEN, JUSSI. Current harmonic compensation in dual three-phase permanent magnet synchronous machines. 2017. Diss.

752. SHI, SHANSHUANG. Development of the EAST articulated maintenance arm and an algorithm study of deflection prediction and error compensation. 2017. Diss.

753. CHEN, JIE. Institutions, social entrepreneurship, and internationalization. 2017. Diss.

754. HUOTARI, PONTUS. Strategic interaction in platform-based markets: An agent-based simulation approach. 2017. Diss.

755. QU, BIN. Water chemistry and greenhouse gases emissions in the rivers of the "Third Pole" / Water Tower of Asia". 2017. Diss.

756. KARHU, PÄIVI. Cognitive ambidexterity: Examination of the cognitive dimension in decision-making dualities. 2017. Diss.

757. AGAFONOVA, OXANA. A numerical study of forest influences on the atmospheric boundary layer and wind turbines. 2017. Diss.

758. AZAM, RAHAMATHUNNISA MUHAMMAD. The study of chromium nitride coating by asymmetric bipolar pulsed DC reactive magnetron sputtering. 2017. Diss.

759. AHI, MOHAMADALI. Foreign market entry mode decision-making: Insights from real options reasoning. 2017. Diss.

760.   AL HAMDI, ABDULLAH. Synthesis and comparison of the photocatalytic activities of antimony, iodide and rare earth metals on SnO2 for the photodegradation of phenol and its intermediates under UV, solar and visible light irradiations. 2017. Diss.

761.   KAUTTO, JESSE. Evaluation of two pulping-based biorefinery concepts. 2017. Diss.

762.   AFZALIFAR, ALI. Modelling nucleating flows of steam. 2017. Diss.

763.   VANNINEN, HEINI. Micromultinationals - antecedents, processes and outcomes of the multinationalization of small- and medium-sized firms. 2017. Diss.

764.   DEVIATKIN, IVAN. The role of waste pretreatment on the environmental sustainability of waste management. 2017. Diss.

765.   TOGHYANI, AMIR. Effect of temperature on the shaping process of an extruded wood-plastic composite (WPC) profile in a novel post-production process. 2017. Diss.

766.   LAAKKONEN, JUSSI. An approach for distinct information privacy risk assessment. 2017. Diss.

767.   KASURINEN, HELI. Identifying the opportunities to develop holistically sustainable bioenergy business. 2017. Diss.

768.   KESKISAARI, ANNA. The impact of recycled raw materials on the properties of wood-plastic composites. 2017. Diss.

769.   JUKKA, MINNA. Perceptions of international buyer-supplier relational exchange. 2017. Diss.

770.   BAYGILDINA, ELVIRA. Thermal load analysis and monitoring of doubly-fed wind power converters in low wind speed conditions. 2017. Diss.

771.   STADE, SAM. Examination of the compaction of ultrafiltration membranes with ultrasonic time-domain reflectometry. 2017. Diss.

772.   KOZLOVA, MARIIA. Analyzing the effects of a renewable energy support mechanism on investments under uncertainty: case of Russia. 2017. Diss.

773.   KURAMA, ONESFOLE. Similarity based classification methods with different aggregation operators. 2017. Diss.

774.   LYYTIKÄINEN, KATJA. Removal of xylan from birch kraft pulps and the effect of its removal on fiber properties, colloidal interactions and retention in papermaking. 2017. Diss.

775.   GAFUROV, SALIMZHAN. Theoretical and experimental analysis of dynamic loading of a two-stage aircraft engine fuel pump and methods for its decreasing. 2017. Diss.

776.   KULESHOV, DMITRII. Modelling the operation of short-term electricity market in Russia. 2017. Diss.

777.   SAARI, JUSSI. Improving the effectiveness and profitability of thermal conversion of biomass. 2017. Diss.

778.   ZHAO, FEIPING. Cross-linked chitosan and β-cyclodextrin as functional adsorbents in water treatment. 2017. Diss.